CHARACTERIZATION OF THE INTERACTIONS OF HYDROGEN, NITROGEN AND OXYGEN WITH SILICON AND III-V SEMICONDUCTOR SURFACES

By

CHERYL FOX CORALLO

A DISSERTATION PRESENTED TO THE GRADUATE SCHOOL
OF THE UNIVERSITY OF FLORIDA IN
PARTIAL FULFILLMENT OF THE REQUIREMENTS
FOR THE DEGREE OF DOCTOR OF PHILOSOPHY

UNIVERSITY OF FLORIDA

1987

ACKNOWLEDGEMENTS

I would like to express my appreciation to Dr. Gar Hoflund for his endless support and assistance. In his capacity as research advisor he was outstanding. Beyond educational and financial support he was instrumental in my growing appreciation of the "gourmet experience." I would also like to thank Greg Corallo for the support he provided and much, much more. Additionally, I would like to thank my parents, Frank and Elaine Fox, for the myriad of things they have done for me which go well beyond words.

Financial support for the research presented in this dissertation was provided by the National Science Foundation, the Petroleum Research Fund administered by the American Chemical Society, the Air Force Office for Scientific Research, a Women Entering Non-Traditional Fields fellowship administered by the Graduate School and the Department of Chemcial Engineering. Thanks go to Perkin-Elmer Physical Electronics in Eden Prairie, MN, at which a portion of the data presented was obtained. I would also like to thank Cerametals Inc. and Showa Denko K. K. for furnishing the InP(111) samples through Sumitomo Electric U.S.A. Inc.

TABLE OF CONTENTS

		PAGE
ACKNOWLEDGEMENTS		ii
LIST OF FIGURES		v
ABSTRACT		viii
CHAPTERS		
I	GENERAL INTRODUCTION	1
II	AN ENERGY-RESOLVED, ELECTRON-STIMULATED DESORPTION STUDY OF HYDROGEN FROM CLEANED AND OXIDIZED Si(100)	5
	Introduction	5
	Experimental	7
	Results and Discussion	8
	Conclusions	22
III	AN ION SCATTERING SPECTROSCOPY AND TEMPERATURE-PROGRAMMED DESORPTION STUDY OF THE INTERACTION OF N_2 WITH Si(111)	23
	Introduction	23
	Experimental	24
	Results and Discussion	26
	Adsorption	26
	Desorption	31
	Conclusions	38
IV	AN ELECTRON-STIMULATED DESORPTION STUDY OF THE INTERACTION OF HYDROGEN, DEUTERIUM AND OXYGEN WITH GaAs(100)	40
	Introduction	40
	Experimental	45
	Results and Discussion	48
	Conclusions	61

PAGE

V A CHARACTERIZATION STUDY OF THE NATIVE OXIDE LAYER FORMED ON CHEMICALLY ETCHED InP(111)..... 63

Introduction..... 63
Experimental..... 66
Results and Discussion..... 67
Conclusions..... 80

VI GENERAL CONCLUSIONS AND RECOMMENDATIONS FOR FUTURE RESEARCH..... 82

REFERENCES..... 85

BIOGRAPHICAL SKETCH..... 95

LIST OF FIGURES

FIGURE		PAGE
2-1	ISS spectra taken from (a) the cleaned sample and (b) a sample exposed to 2000 L of O_2 at 400 °C	10
2-2	ESD mass spectrum taken from the cleaned Si(100) surface corresponding to figure 2-1(a)	11
2-3	H^+ energy distribution spectra taken from (a) the cleaned sample and (b) the sample following exposure to a 240 eV electron beam for 20 minutes and a 400 eV beam for 15 minutes	13
2-4	H^+ energy distribution spectra taken from (a) the electron-beam-exposed sample shown in figure 2-3(b), and (b) the beam-exposed sample which had been annealed at 650 °C for 15 minutes. The ordinates of (a) and (b) are scaled relatively to one another	15
2-5	Angle-resolved, energy-resolved ESD spectra obtained from a cleaned surface for (a) H^+ desorbing normal to the surface and (b) H^+ desorbing at 45° with respect to the sample surface plane.	17
2-6	H^+ energy distribution spectra obtained from (a) a sample exposed to 2000 L of O_2 at 400 °C and (b) the cleaned sample (same as figure 2-3(a)).	19
2-7	The upper portions of the H^+ energy distribution spectra taken from (a) the cleaned surface, (b) a surface exposed to a 240 eV electron beam for 30 minutes, (c) a surface exposed as in (b) with an additional exposure to a 400 eV beam for 25 minutes, (d) the beam-exposed surface in (c) followed by a 400 °C anneal for 15 minutes and (e) the beam-exposed surface followed by a 950 °C anneal for 10 minutes.	21

PAGE

3-1 ISS spectrum taken from a Si(111) surface which had been exposed to 75 L of N_2 at room temperature. For a scattering angle of 73° E_1/E_0 is 0.70 for N and 0.79 for Si. All ISS data were taken at room temperature using 1 keV helium ions..... 27

3-2 Ratio of N ISS peak heights to that of Si as a function of room temperature N_2 exposure..... 28

3-3 Typical TPD spectra for masses (a) 14, (b) 28 and (c) 29 for a sample which had been exposed to 1000 L of N_2 at room temperature. The ordinates of (a), (b) and (c) are not scaled relatively to one another. The experimental peak area ratios are $(a(T_1)):(a(T_2)):(b):(c) = 1:3.5:44.3:6.1$..... 32

3-4 TPD spectra for a sample which had been exposed to 1000 L of N_2 at room temperature. Spectra labeled (a) refer to the desorption of H_2 and (b) refers to the desorption of H. The data in (A) were taken from a sample with a different history than the sample in (B) (see text)..... 36

4-1 AES spectrum (a) of contaminated GaAs(100) taken after solvent cleaning and (b) taken after the IBA cleaning procedure..... 47

4-2 ESD mass spectrum taken from the contaminated surface corresponding to figure 4-1(a). All ESD spectra were taken using a primary beam energy of 140 eV..... 50

4-3 ESD mass spectrum taken after exposing the clean GaAs surface corresponding to figure 4-1(b) to a dose of 2000 L of D_2 while heating the sample at 200 °C..... 53

4-4 ESD spectra corresponding to the mass spectrum shown in figure 4-3. (a) Total-ion (H^+ and D^+) energy distribution spectrum and ESDIED spectra of (b) H^+ and (c) D^+..... 55

4-5 AES spectrum taken from GaAs(100) after a dose of 12,000 L of O_2 at room temperature..... 57

PAGE

4-6 ESD spectra taken after exposing the oxidized surface corresponding to figure 4-5 to 2000 L of D_2 while heating the sample at 200 °C. (a) Total-ion (H^+ and D^+) energy distribution spectrum and ESDIED spectra of (b) H^+ and (c) D^+..... 59

4-7 ESD mass spectra taken (a) at an ion kinetic energy of 0.8 eV and (b) at an ion kinetic energy of 3.5 eV..... 60

5-1 ISS spectrum of air-exposed InP(111)..... 68

5-2 Angle-integrated AES spectrum of the same surface shown in figure 5-1..... 70

5-3 AES spectra of the In $M_{4,5}N_{45}N_{45}$ features taken from the same surface shown in figure 5-2. Spectra (a) and (c) were taken at exit angles of 10° and 85° respectively. Spectrum (b) is angle integrated over all exit angles..... 71

5-4 XPS spectra of the (A) P 2p and (B) In 3d peaks taken at exit angles of (a) 10° and (b) 85°..... 73

5-5 XPS spectra of the (A) C 1s and (B) O 1s peaks taken at exit angles of (a) 10° and (b) 85°..... 74

5-6 Angle-resolved valence band XPS spectra taken at exit angles of (a) 10° and (b) 85°..... 78

5-7 Angle-integrated AES compositional profile obtained by argon-ion sputtering..... 79

Abstract of Dissertation Presented to the Graduate School
of the University of Florida in Partial Fulfillment of the
Requirements for the Degree of Doctor of Philosophy

CHARACTERIZATION OF THE INTERACTIONS
OF HYDROGEN, NITROGEN AND OXYGEN WITH SILICON AND
III-V SEMICONDUCTOR SURFACES

By

CHERYL FOX CORALLO

December, 1987

Chairman: Gar B. Hoflund
Major Department: Chemical Engineering

The interaction between gases and semiconductors has been studied using ultrahigh vacuum (UHV) surface analytical techniques. Electron-stimulated desorption (ESD) was used to study hydrogen present on cleaned and oxidized Si(100). It is demonstrated by kinetic energy analysis of the hydrogen ions emitted through ESD that multiple states of adsorbed hydrogen are present. Electron beam exposure, annealing and oxygen exposure dramatically alter the sites or binding energy states of hydrogen present on the surface.

Ion scattering spectroscopy (ISS) and temperature-programmed desorption (TPD) were used to investigate the interaction between N_2 and a Si(111)(7x7) surface at room temperature. Adsorbed nitrogen is detected using ISS for doses as low as 2 L (1L = 10^{-6} Torr·sec.) and saturation occurs at 75 L. At least two chemisorbed states of nitrogen are observed using TPD. Hydrogen, originating from the sample bulk, associates with the surface nitrogen. The surface

structure was monitored throughout the N_2 adsorption experiments using low energy electron diffraction (LEED).

The interaction of hydrogen with cleaned and oxidized GaAs(100) was studied using ESD. Deuterium adsorbs on the cleaned and oxidized surfaces for a radiantly heated sample in the range 200-400 °C. Different adsorbed states of hydrogen are observed by kinetic energy analysis of the desorbing ions.

The native oxide layer of a chemically polished and etched InP(111) surface was characterized using Auger electron spectroscopy (AES), angle-resolved X-ray photoelectron spectroscopy (ARXPS) and ISS. The oxide layer is about 30Å thick and forms a sharp interface between the oxide and the bulk InP. The outermost atomic layer is In rich, and the region just below this is P rich. InP and $InPO_3$ exist in approximately equal concentrations in the oxide layer. A small amount of In_2O_3 is also detected. Carbon is present throughout the oxide layer as graphite and/or hydrocarbons.

CHAPTER I
GENERAL INTRODUCTION

The study of the interaction between gases and semiconductors is very important for gaining fundamental knowledge of semiconductor surface properties as well as in terms of understanding and controlling the growth of epitaxial layers and passivating layers on semiconductor surfaces. Numerous studies have been performed to investigate these interactions. However, discrepancies continue to exist and a considerable number of questions remain unanswered.

The focus of the experimental work which is presented here has been to investigate the interaction of gases with Si and III-V (GaAs and InP) semiconductor single crystals. In order to investigate these interactions with minimal contamination effects, the studies were done under ultra-high vacuum (UHV) conditions. The vacuum system used in a majority of the studies presented here has been described previously.[1] (The study for which another vacuum system was used is noted in the text.) Briefly, it consists of a stainless steel chamber, typically at a base pressure of 10^{-10} Torr, with capabilities for performing a wide variety of experimental techniques. Techniques such as X-ray photoelectron spectroscopy (XPS) (also called electron spectroscopy for chemical analysis or ESCA), Auger electron spectroscopy (AES), ion scattering spectroscopy (ISS) and electron-stimulated desorption (ESD) were performed using a double-pass cylindrical mirror analyzer (CMA) equipped with an

internal coaxial electron gun and an angularly resolving movable aperture. Low energy electron diffraction (LEED) patterns were observed using a hemispherical grid system and were recorded by photographing the pattern through a window opposite the hemisphere. Temperature-programmed desorption (TPD) data were obtained using a quadrupole mass spectrometer by recording the intensity of signals of as many as four masses simultaneously as a function of temperature.

The disseration consists of five chapters in addition to the general introduction. Chapters II and III are concerned with the interaction of gases with the (100) and (111) surfaces of Si, respectively. Chapter IV is a study of the interaction of gases with a GaAs(100) surface, and Chapter V is an investigation of an InP(111) surface. Each chapter is a complete individual study. The general conclusions and recommendations for future research are presented in Chapter VI.

More specifically, Chapter II presents results of an energy-resolved ESD study of hydrogen from cleaned and oxidized Si(100). One of the relatively few surface spectroscopies which detects hydrogen directly is ESD. Therefore, it is very useful in studying the interaction between hydrogen and semiconductors. This interaction has both scientific and technological importance particularly due to the fact that hydrogen has been shown to reduce electrical activity in a number of semiconductors.[2-18] Using ESD, it was found that cleaning the surface by ion bombardment and annealing does not completely remove hydrogen from a Si(100) surface. Kinetic energy

analysis of the hydrogen ions emitted through ESD is useful in distinguishing between different adsorbed states of hydrogen. Electron beam exposure, annealing and oxygen exposure dramatically alter the kinetic energy distribution of the desorbing hydrogen ions. Angle-resolved, energy-resolved ESD spectra of H^+ from the cleaned Si(100) surface are also presented which show an angular dependence of the H^+ energy distributions.

The interaction between nitrogen and silicon is also important, particularly since silicon nitride is increasingly being used as an insulatng layer in device production and nitrogen is sometimes present as a background gas during device fabrication.[19] In Chapter III a study is presented in which ISS and TPD were used to study the interaction between N_2 and a Si(111)(7x7) surface at room temperature. ISS provides an excellent means of monitoring the amount of adsorbed species at the surface as a function of exposure due to its high surface sensitivity. Using ISS, the adsorption of nitrogen on Si(111) at room temperature was characterized and a saturation dose was determined. The initial sticking probability was also found. TPD results indicate that at least two chemisorbed states of nitrogen exist. Hydrogen, which originates from the bulk of the sample, associates with the surface nitrogen. LEED was used to monitor surface structure throughout N_2 adsorption and during subsequent heating.

The interaction between GaAs and hydrogen is an important topic which has been discussed in relatively few studies. The results of

an ESD study of the interaction of hydrogen and deuterium with cleaned and oxidized GaAs(100) are presented in Chapter IV. Cleaning the surface by ion bombardment and annealing does not completely remove hydrogen from the surface so dosing was performed using deuterium. It was verified that molecular deuterium does not adsorb at significant rates at room temperature on the cleaned or oxidized surface, but it does adsorb on both surfaces when the sample is subjected to radiant heating in the range 200-400 °C with a tungsten filament. ESD gives a semiquantitative relative measure of the amount of adsorbed deuterium, and kinetic energy analysis of the desorbing ions is useful in distinguishing between different adsorbed states of hydrogen.

InP is becoming an important III-V semiconductor material for the fabrication of semiconductor devices.[20-23] Chapter V consists of a characterization study of the native oxide layer formed on chemically polished and etched InP(111) by exposure to air. ISS was used to determine the composition of the outermost surface layer, and angle-resolved XPS and depth profiling using Ar^+ and AES give the composition of the oxide layer. The thickness of the oxide layer and the relative amount of the species present in this layer were also determined.

CHAPTER II
AN ENERGY RESOLVED, ELECTRON-STIMULATED DESORPTION STUDY OF HYDROGEN FROM CLEANED AND OXIDIZED Si(100)

Introduction

An understanding of the interaction between hydrogen and semiconductors has both technological and scientific importance. Hydrogen has been shown to reduce electrical activity in silicon,[2-12] germanium[13] and gallium arsenide.[14-18] For example, Benton et al.[3] achieved hydrogen passivation of electrically active defects created during laser annealing of crystalline silicon by exposure to atomic hydrogen in a hydrogen plasma. Pearton and Tavendale[4] showed that both the deep donor and acceptor levels associated with gold are passivated by exposing silicon samples to a hydrogen plasma. Mechanisms responsible for hydrogen passivation in silicon have been proposed by a number of authors.[5-9,11,24,25]

In addition to the interest in the passivation effects of hydrogen, the interaction of hydrogen and silicon has been studied in order to gain a better understanding of the surface geometry of reconstructed clean silicon surfaces.[26-31] The ease with which hydrogen induces surface reconstructions on the low-index planes of silicon has been used to evaluate the various models for reconstruction of the clean surface. For example, Norton[30] found that changes in the diffraction pattern induced by adsorption of hydrogen on Si(001) are consistent with the asymmetric dimer model as

opposed to the symmetric dimer model. Numerous calculations of surface electronic properties have also been carried out for both clean and hydrogen-exposed silicon surfaces,[27,32-40] and a variety of experimental studies of the silicon/hydrogen system have been performed.[26,29,31,41-66] These studies show that several surface species (including mono-, di- and trihydrides) can exist depending upon sample history and exposure conditions.

Relatively few surface analytical techniques detect hydrogen directly due to its light mass, small cross section for many processes and lack of core-level electrons. However, ESD is highly sensitive to hydrogen because it is a mass spectrometric technique. ESD is powerful in that it can yield information on surface bonding structure and/or mechanisms of excitation and desorption. Few ESD studies of the silicon/hydrogen system have been published. Madden et al.[56] correlated the threshold for electron- and photon-stimulated desorption with a localized Auger final state for atomically adsorbed hydrogen on Si(100). ESD was also used in a study by Kazmerski[67] to investigate the interaction of hydrogen ions at grain boundaries in polycrystalline silicon.

In the present study ESD is used to examine the binding states of hydrogen present on Si(100). Hydrogen is found to be present on both the cleaned and oxygen-exposed Si(100) surfaces and energy distributions of desorbing H^+ from cleaned and oxygen-exposed surfaces are presented. The effects of electron beam exposure and annealing on the H^+ energy distributions are also discussed.

Additionally, angle-resolved and energy-resolved ESD spectra of H^+ from the cleaned Si surface are presented.

Experimental

A polished Si(100) single crystal was used in this study. The sample was ultrasonically cleaned in electronic grade trichloroethylene, acetone and methanol and then rinsed with deionized water prior to insertion into the vacuum chamber. The Si was heated radiantly to 700 °C by a tungsten filament placed directly behind the sample, and heating above 700 °C was accomplished using electron bombardment. The temperature of the sample was monitored using an optical pyrometer. The sample was cleaned using cycles of ion bombardment and annealing (IBA) at 950 °C until a distinct (2x1) LEED pattern was obtained and the ISS oxygen signal was no longer detected. The oxygen signal was below the AES detection limit before it was below the ISS detection limit.

The vacuum system (base pressure of 2×10^{-10} Torr) used in these experiments has been described previously.[1] ESD, AES and ISS were performed using a double-pass cylindrical mirror analyzer (CMA) (PHI Model 15-255 GAR) equipped with an internal coaxial electron gun and an angularly resolving movable aperture. The sample was positioned at an angle of 45° with respect to the CMA axis. AES and ISS data were taken by operating the CMA in the nonretarding mode. The details of the data collection are given elsewhere.[68] LEED patterns were observed using a PHI Model 15-180 hemispherical grid system.

ESD data were taken using the CMA as a time-of-flight mass spectrometer.[69] Energy analysis of low-energy (less than 20 eV) positive ions was accomplished by operating the CMA in the retarding mode with a pass energy of 80 eV. The ions were first accelerated by a negative potential placed on the second grid and inner cylinder. The outer cylinder was maintained at a more positive potential (but negative with respect to ground) than the inner cylinder. The complete set of CMA operating voltages has been published previously.[70] For mass analysis the electron beam was pulsed onto the sample for 300 ns and pulses were counted for 300 ns after an appropriate delay period (5.5 μs for H^+). A primary beam energy of 240 eV and a primary beam current of approximately 500 nA were used. The mass spectrum of the desorbing ions was obtained by selecting an ion kinetic energy and scanning the delay time. An electron-stimulated desorption-ion energy distribution (ESDIED) spectrum was obtained by scanning the ion kinetic energy with the CMA. H^+ was the only species found to desorb by ESD in this study. Therefore, time gating was not necessary to obtain the energy distributions of the hydrogen ions.

Results and Discussion

In ESD electrons impact a surface creating localized excitations which decay causing desorption of ions, neutrals and metastable species. These low energy ions can desorb only from the top atomic layer because ions which are created beneath the top monolayer have a

high probability of being neutralized during the desorption process. However, excitations created beneath the surface can emit secondary electrons which may create excitations at the surface resulting in emission of ions.[71] Thus, ESD is highly surface sensitive with respect to the emitted ionic signal but not as surface specific with respect to the primary electron beam.

The ISS spectrum shown in figure 2-1(a) was taken from a sample cleaned by IBA cycles followed by a 950 °C anneal. Only a silicon peak is observed in this ISS spectrum. Also, an AES spectrum (not shown) and a distinct (2x1) LEED pattern characteristic of the clean Si(100) surface were obtained from this surface. The ESD mass spectrum corresponding to figure 2-1(a) is shown in figure 2-2. It is obvious from this spectrum that hydrogen is present on the Si(100) surface which was cleaned by IBA cycles. The amount of hydrogen present on this silicon surface is not known because the total ESD cross sections for hydrogen on Si(100) are not known and an independent means of measuring surface hydrogen concentration was not available. It is difficult to determine the surface concentration of hydrogen since relatively few techniques directly detect hydrogen and these techniques are difficult to quantify. For example, Madden[54] has shown that changes in the lineshape on the low energy side of the Si $L_{2,3}VV$ AES peak are induced by hydride formation. However, the AES sensitivity factor for hydrogen is not known so quantifying the amount present is not possible using AES. Although the amount of hydrogen present is not known, ESD provides considerable information about the adsorbed states of hydrogen.

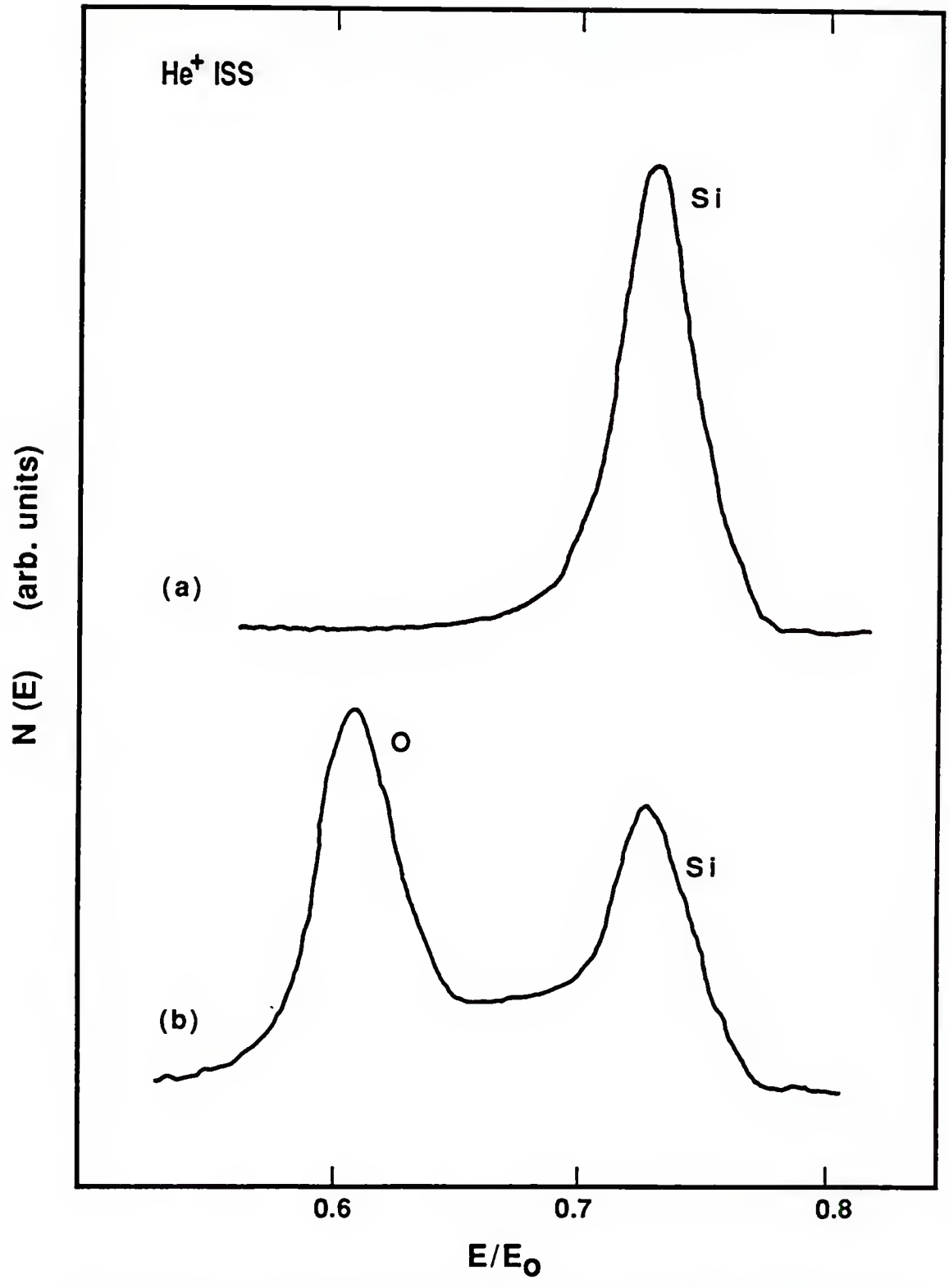

Figure 2-1. ISS spectra taken from (a) the cleaned sample and (b) a sample exposed to 2000 L of O_2 at 400 °C.

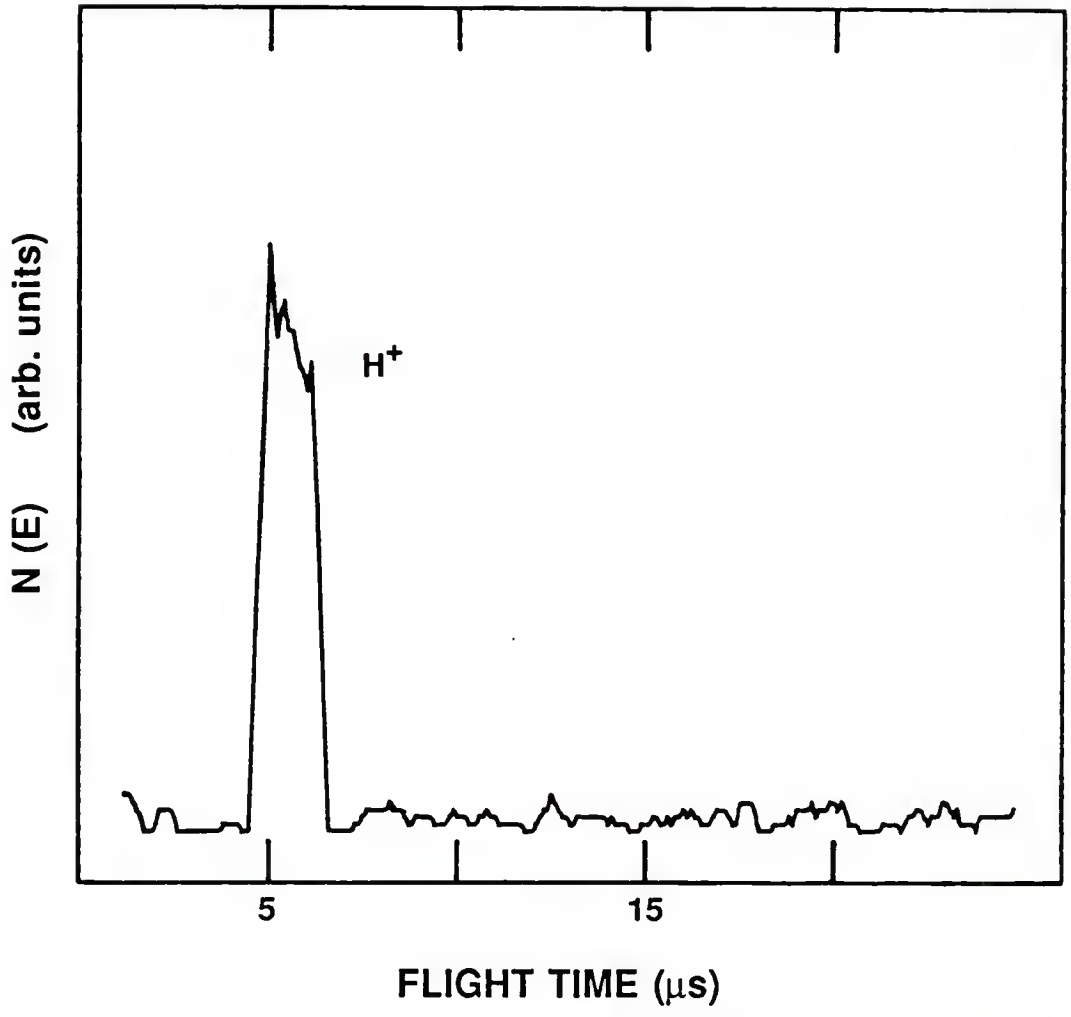

Figure 2-2. ESD mass spectrum taken from the cleaned Si(100) surface corresponding to figure 2-1(a).

In most cases different peaks in an energy distribution spectrum are due to different desorbing states. However, complexities such as differing cross sections for desorption from different states or desorption by more than one mechanism can make ESDIED spectra more difficult to interpret. A review of ESDIED which covers the experimental methods, ESD mechanisms and theory and addresses the topics of ESD cross sections, desorption by more than one mechanism and desorption from defect sites has been published by Hoflund.[70] These topics are not discussed in detail in this paper.

An interesting effect on the energy distribution of the desorbing ions was found to occur upon exposure of the sample to the electron beam. The total ion (H^+) energy distributions taken from (a) the cleaned sample and (b) the same sample following collection of 33 ESD spectra (primary beam energy of 240 eV for 20 minutes) and further exposure to a 400 eV beam for 15 minutes is shown in figure 2-3. Electron beam exposure results in a depopulation of the states which desorb at higher kinetic energy implying that they have larger desorption cross sections. This effect was also observed for less severe beam exposures. However, the depopulation is less dramatic in these cases. This implies that the features in the energy distribution are due to desorption from different sites or binding energy states with different desorption cross sections.

It was found that the higher energy states could be repopulated with hydrogen by annealing. Energy distributions taken from (a) the electron-beam-exposed sample shown in figure 2-3(b), and (b) the

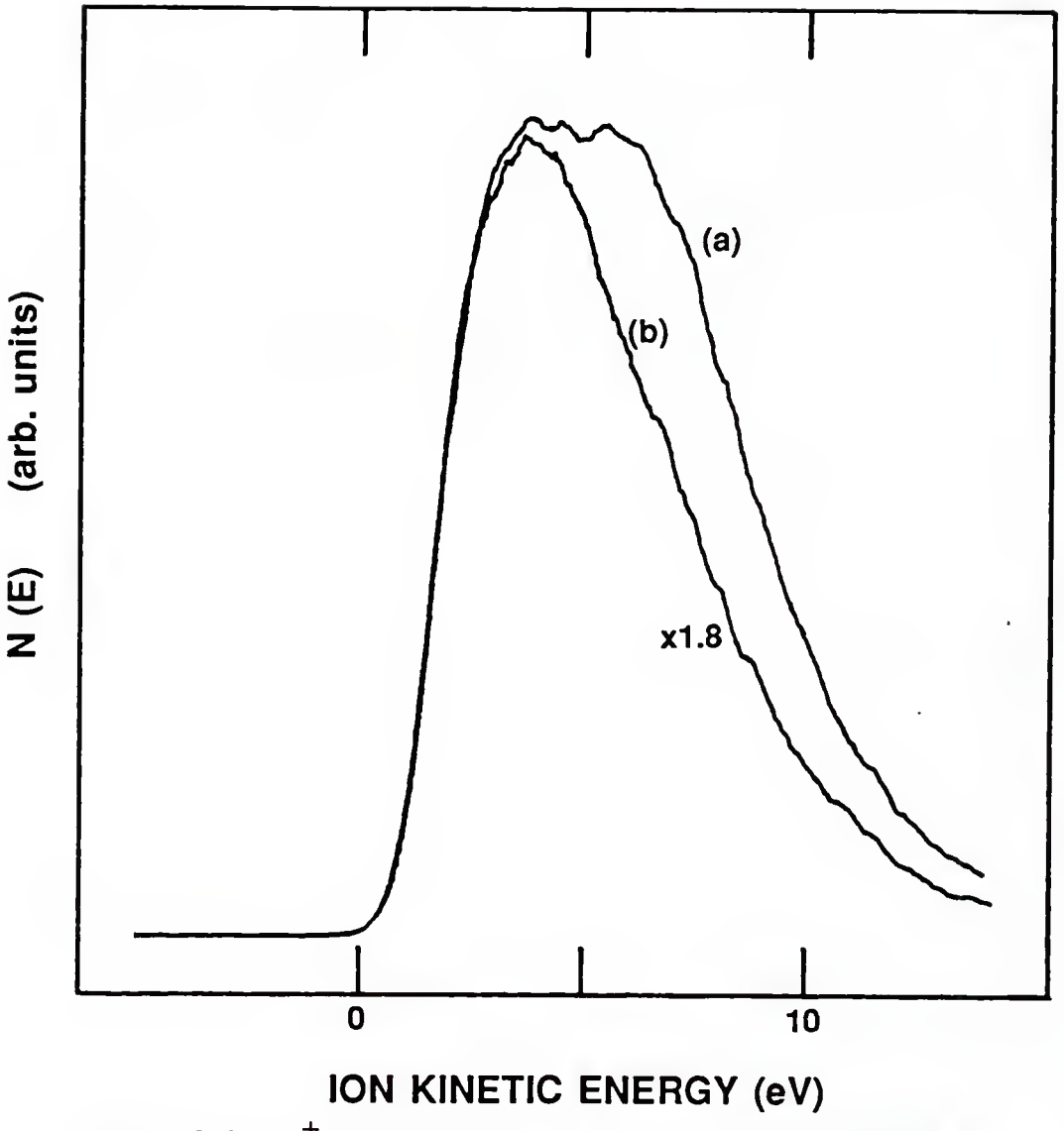

Figure 2-3. H^+ energy distribution spectra taken from (a) the cleaned sample and (b) the sample following exposure to a 240 eV electron beam for 20 minutes and a 400 eV beam for 15 minutes.

beam-exposed sample following a 15 minute anneal at 650 °C are shown in figure 2-4. The energy-resolved ESD spectrum following annealing closely resembles spectrum 2-3(a) except for the small features present on the top of the energy distribution spectra which are discussed in more detail below. For less severe beam exposures and correspondingly lessened depopulation of the higher energy states, annealing temperatures as low as 400 °C are sufficient to repopulate these states at reasonable rates.

An attempt was also made to adsorb deuterium on the Si(100) surface under various conditions. In agreement with previous studies,[29,54] D_2 does not adsorb appreciably at room temperature on a clean Si(100) surface. Furthermore, D^+ was not detected by ESD following D_2 exposures of 1000 to 3000 L (1L = 10^{-6} Torr·sec.) at dosing temperatures of 400, 500 or 600 °C.

Both of the facts that annealing the silicon repopulates surface hydrogen states and that D_2 does not adsorb on Si(100) imply that the source of the surface hydrogen detected by ESD is hydrogen in the silicon bulk which diffuses to the surface during annealing. The presence of molecular and atomic hydrogen in the Si lattice is discussed in a paper by Corbett et al.[72]

Electron-stimulated desorption-ion angular distribution (ESDIAD) experiments are often capable of yielding bonding structural information,[70] but it is usually not possible to obtain the energy distributions of ions desorbing at particular angles using typical ESDIAD experimental configurations. It is expected that ions which

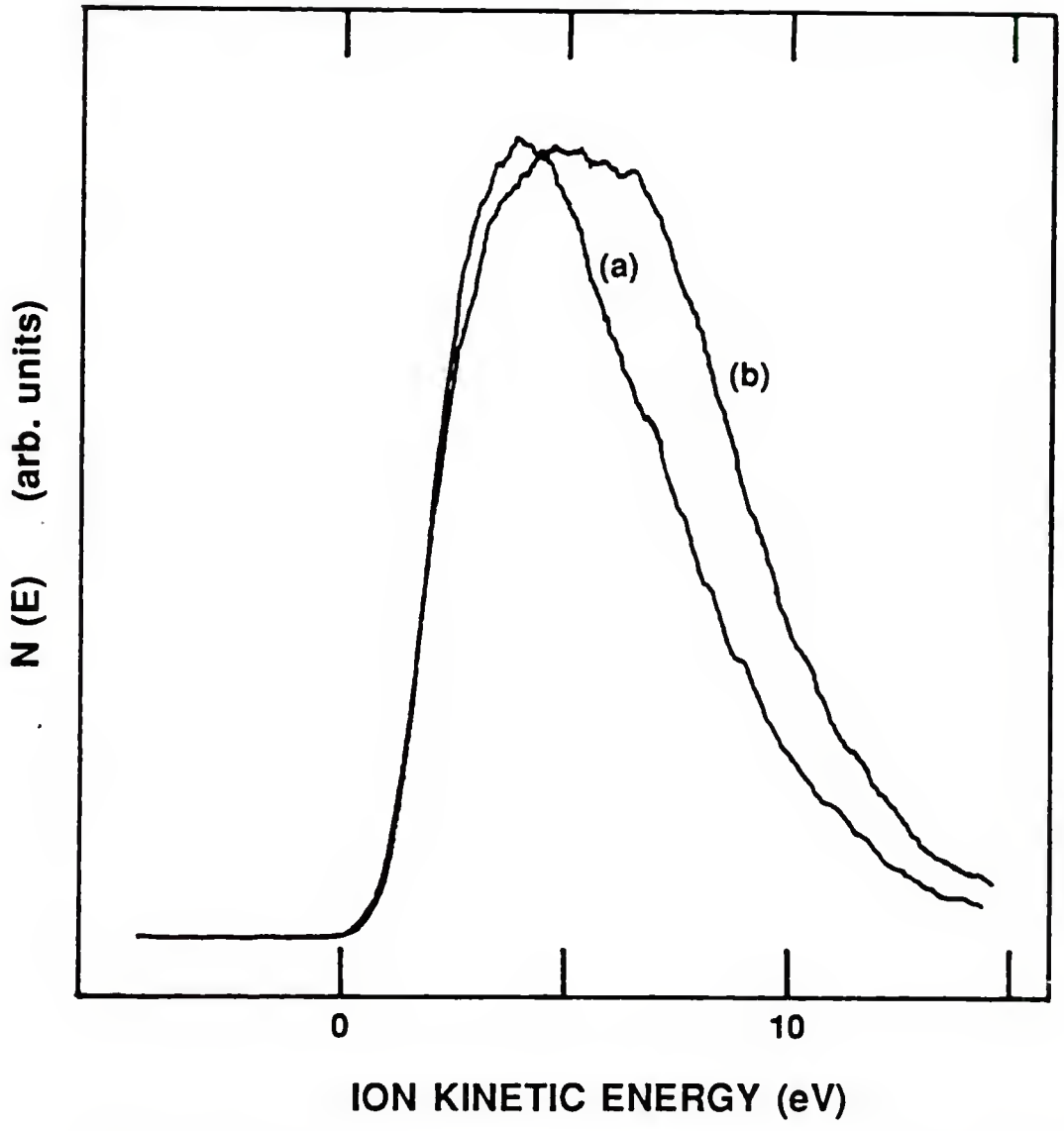

Figure 2-4. H^+ energy distribution spectra taken from (a) the electron-beam-exposed sample shown in figure 2-3 (b), and (b) the beam-exposed sample which had been annealed at 650 °C for 15 minutes. The ordinates of (a) and (b) are scaled relatively to one another.

desorb with different angular distributions from different sites or binding states would also have different energy distributions. This hypothesis was tested using the 12° aperture of the CMA to collect ions which desorbed at different angles with respect to the surface. The resulting angle-resolved, energy-resolved ESD spectra are shown in figure 2-5. Spectrum (a) consists of H^+ desorbing in the direction normal to the surface, and spectrum (b) consists of ions desorbing at approximately 45° with respect to the sample surface plane (in the $(\bar{1}\bar{1}1)$ direction relative to the bulk silicon). The signal for the H^+ desorbing normal to the surface is similar in intensity to that of the H^+ desorbing at an angle of 45°. It is apparent from these spectra that H^+ energy distributions are angular dependent providing further evidence that multiple states of adsorbed hydrogen are present on the cleaned Si(100) surface. In fact, spectrum (a) appears to consist of at least two peaks while the lower-energy feature is absent in spectrum (b). Hydrogen was detected at all angles which were examined (approximately 15°, 45°, 60° and 90° with respect to the sample surface plane). The signal intensity for H^+ desorbing at 60° is similar to that of H^+ desorbing at 45° and 90°, but the signal intensity for H^+ desorbing at 15° is less than half of the signal intensity obtained at the other angles. The energy distribution for hydrogen desorbing at 60° is very similar to the distribution for normal desorption, while the distribution for H^+ desorbing at 15° resembles that of H^+ desorbing at 45°.

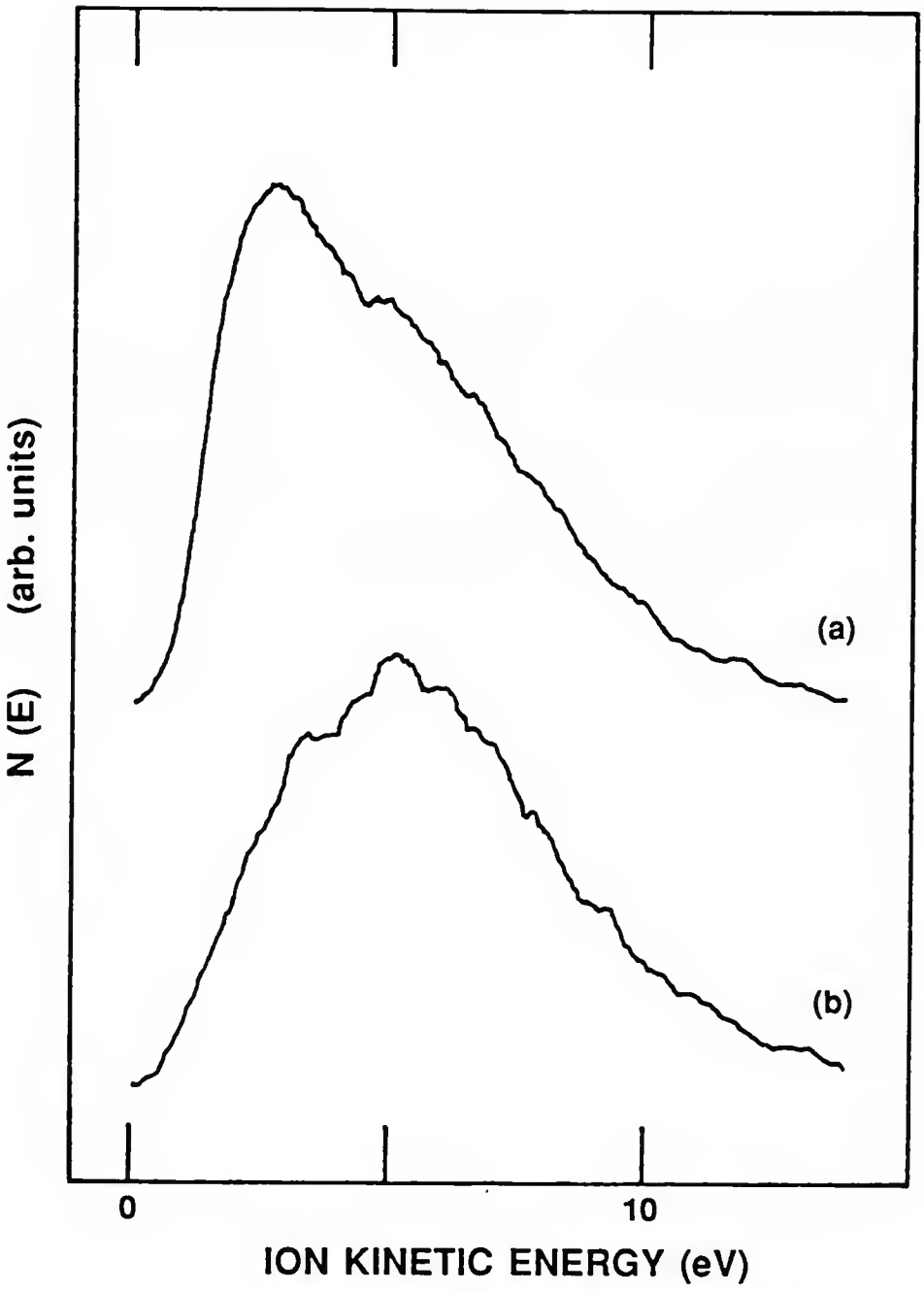

Figure 2-5. Angle-resolved, energy-resolved ESD spectra obtained from a cleaned surface for (a) H^+ desorbing normal to the surface and (b) H^+ desorbing at 45° with respect to the sample surface plane.

In order to investigate the effect that the presence of oxygen has on the surface hydrogen, the sample was annealed at 950 °C for 5 minutes and then dosed with 2000 L of O_2 at 400 °C. The ISS spectrum obtained from this oxygen-exposed surface is shown in figure 2-1(b). Following the oxygen exposure, the O ISS signal is 1.3 times that of the Si signal. From scattering cross section estimates, there are more than twice as many O atoms on this surface as Si atoms. An ESD mass spectrum taken after the oxygen exposure reveals that H^+ is the only ionic species which desorbs from this surface (i.e., no oxygen or hydroxyl ions are detected). The ESD ion energy distribution spectrum obtained from this surface is shown in figure 2-6(a). The spectrum shown in figure 2-6(b) is the same as that shown in figure 2-3(a) taken from the cleaned, annealed surface. The hydrogen ions desorb from the oxygen-dosed surface with a much narrower energy distribution than from the cleaned surface. The higher energy states are depopulated for the oxygen-exposed surface; even more so than for the electron-beam-exposed surface. It is possible that this narrow energy distribution is due to desorption from one well-defined state such as hydrogen bonded in the form of hydroxyl groups. The formation of hydroxyl groups has been shown to occur upon hydrogen-ion exposure at oxygen-rich grain boundaries in polycrystalline Si by Kazmerski[67] using ESD, SIMS and TPD. Using high resolution electron energy loss spectroscopy (HREELS), Nishijima et al.[65] determined that SiH and SiOH species form on the Si(111)(7x7) surface following exposure to H_2O at 300 K. However,

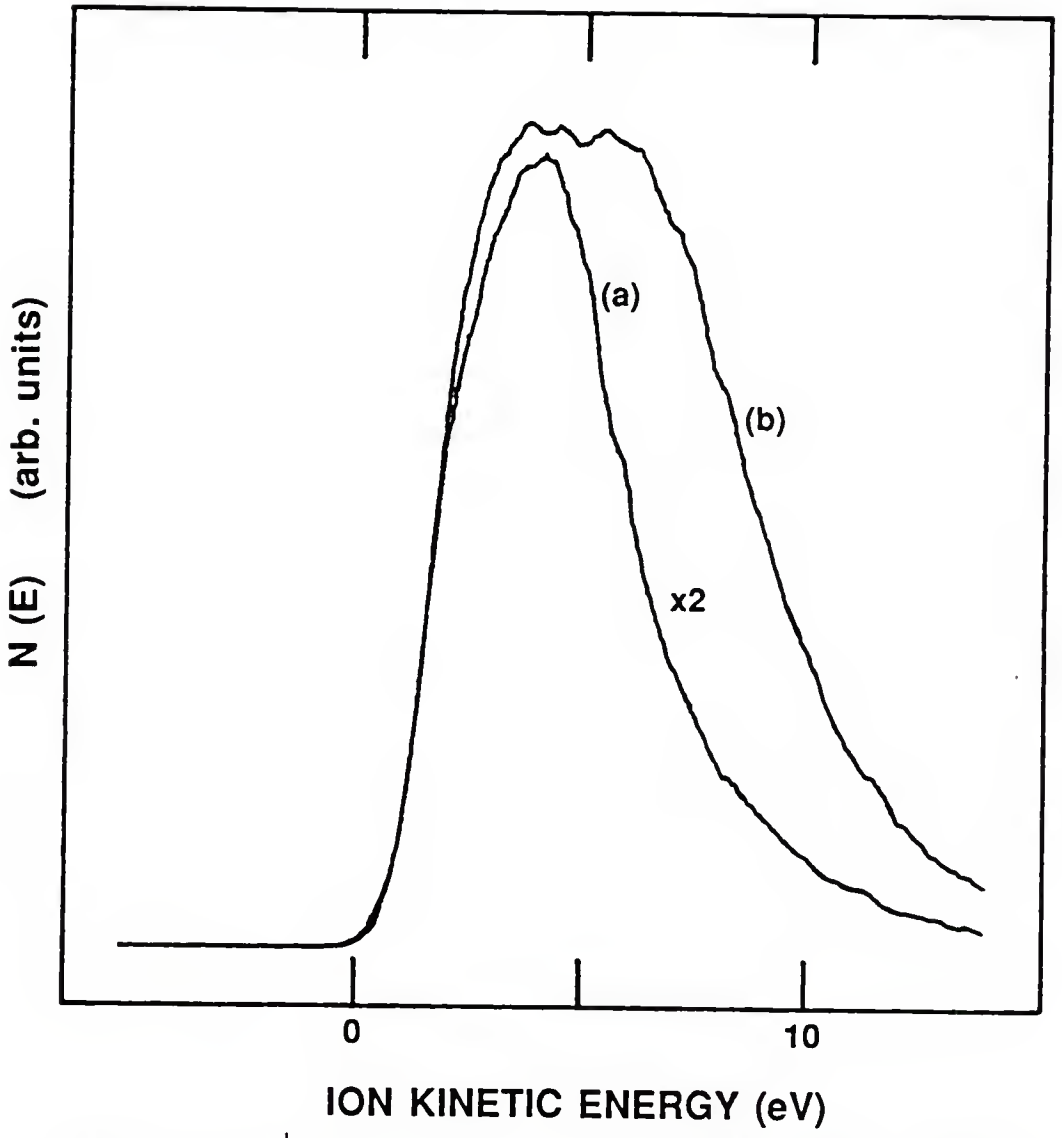

Figure 2-6. H^+ energy distribution spectra obtained from (a) a sample exposed to 2000 L of O_2 at 400 °C and (b) the cleaned sample (same as figure 2-3(a)).

other possibilities exist which could explain the ESD data. It may be that the hydrogen desorbing from the oxygen-exposed surface is bonded as on the cleaned surface but that the higher energy desorption states are no longer able to desorb by ESD due to an interaction with oxygen or that the higher energy states are no longer present on the surface. More information is required to specify the forms of the hydrogen at the Si(100) surface.

The presence of small features on the top of the ESDIED spectra was observed during the course of this study. For a cleaned surface which had been annealed at 950 °C, there are four primary features on the ESDIED spectra and a shoulder on the high energy side (figure 2-7(a)). Electron beam exposure results in slight shifts in the energy of these features and a slight depopulation of the higher energy states relative to the lowest energy state. This can be seen in figure 2-7(b) for a surface exposed to a 0.5 μA, 240 eV electron beam for 30 minutes. The results of additional beam exposure are illustrated in figure 2-7(c). This spectrum was obtained following exposure to a 240 eV beam for 30 minutes and a 400 eV beam for 25 minutes. There is a further depopulation of the higher energy states. Annealing the beam-exposed surface results in repopulation of the higher energy states as has been discussed previously. However, the primary small features are not well defined for annealing temperatures of 650 °C and below. Figure 2-7(d) was obtained from a sample which had been annealed to 400 °C. Upon annealing to 950 °C the well-defined small features are again present (figure 2-

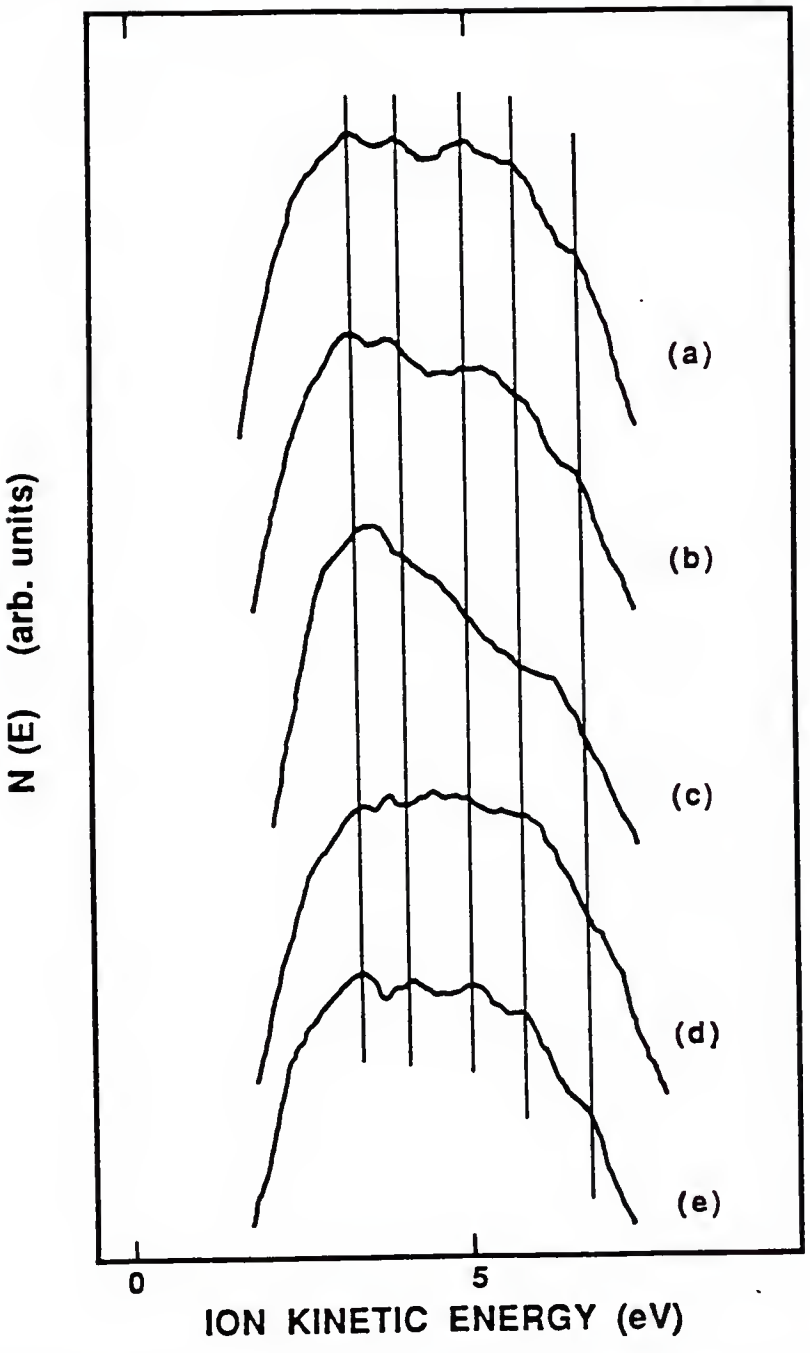

Figure 2-7. The upper portion of the H^+ energy distribution spectra taken from (a) the cleaned surface, (b) a surface exposed to a 240 eV electron beam for 30 minutes, (c) a surface exposed as in (b) with an additional exposure to a 400 eV beam for 25 minutes, (d) the beam-exposed surface in (c) followed by a 400 °C anneal for 15 minutes and (e) the beam-exposed surface followed by a 950 °C anneal for 10 minutes.

7(e)). It is possible that the individual small features are due to desorption from distinct adsorbed states of hydrogen on the surface.

Conclusions

ESD has been used to investigate the hydrogen adsorbed on a cleaned and an oxidized Si(100) surface. IBA cleaning cycles do not remove the surface hydrogen completely. The hydrogen detected using ESD diffuses to the surface from the bulk of the Si sample during annealing and is not due to adsorption of gas-phase hydrogen. Energy distributions of the desorbing H^+ provide information about the adsorbed states of hydrogen on the surface. Electron beam exposure results in a depopulation of the higher energy states which are repopulated upon annealing. Exposure to oxygen results in a narrowing of the energy distribution and a more marked depopulation of the higher energy states. Angle-resolved, energy-resolved ESD provides further evidence that multiple states of adsorbed hydrogen are present on the cleaned Si(100) surface.

CHAPTER III
AN ION SCATTERING SPECTROSCOPY AND TEMPERATURE-PROGRAMMED DESORPTION STUDY OF THE INTERACTION OF N_2 WITH Si(111)

Introduction

The importance of very thin insulating layers in the production of VLSI (very large scale integration) devices is evident. Silicon nitride is increasingly being used instead of the oxide for this purpose.[19] As device down-scaling continues, a thorough understanding of the chemical, physical and electronic properties of insulating films becomes even more important. In addition, nitrogen is sometimes present as a background gas during device fabrication. For these reasons it is essential to understand the interaction between nitrogen and silicon.

A number of studies have been done on films produced by chemical vapor deposition (CVD) using SiH_4 combined with NH_3,[73-76] NH_3/N_2O,[77] and NH_3/NO.[78,79] Relatively high pressure (0.1-760 Torr) nitridation of Si using N_2 or NH_3 has also been studied.[80-88] However, in order to study the initial stages of growth of thin nitride films on Si with minimal contamination effects, the study must be done under ultrahigh vacuum (UHV). Investigations have been reported in which Si is exposed to various nitriding gases such as: N,[89-93] N^+,[91,94] N_2,[95-97] NH_3,[92,95,98-100] NO[97,101,102] and N_2O[103] under UHV conditions. The majority of these studies have focused on thermal nitridiation and have shown that an (8x8) or a quadruplet surface is

formed on Si(111) depending upon the cleanliness and temperature of the sample as well as the nitriding gas pressure. It has been suggested that the quadruplet pattern is evidence of the formation of a Si_3N_4 surface layer.[89-91,95,98,99]

Relatively few room temperature studies have been reported, particularly concerning the interaction of Si with N[90,93] or N_2.[95,97] Heckingbottom[95] found only a slight deterioration of the Si(111)(7x7) pattern with a room temperature N_2 exposure at 10^{-6} Torr while Wiggins et al.[97] were unable to detect any adsorbed nitrogen using AES for N_2 exposures at 10^{-6} Torr for 5 minutes and sample temperatures below 600 °C. However, it is demonstrated in the present study using ISS and TPD that N_2 does adsorb on Si(111) under these conditions.

Experimental

A polished, n-type (P-doped) Si(111) single crystal was used in this study. The resistivity of the sample was 5-30 ohm·cm. The sample (17.5 x 9 x 0.5 mm) was ultrasonically cleaned in electronic grade trichloroethylene, acetone and methanol and then rinsed with deionized water prior to insertion into the vacuum chamber. The Si was mounted in a tungsten frame and heated radiantly to 700 °C by a tungsten filament placed directly behind the sample. Heating above 700 °C was accomplished using electron bombardment. The temperature of the sample was monitored using an optical pyrometer. The sample was cleaned using cycles of ion bombardment followed by annealing

(IBA) until a distinct (7x7) LEED pattern was obtained and the ISS oxygen signal was minimized. The sample was cleaned by annealing at 920 °C for at least five minutes between the repeated N_2 exposures during TPD experiments.

The vacuum system (base pressure of 10^{-10} Torr) used in these experiments has been described previously.[1] ISS and AES were performed using a double-pass cylindrical mirror analyzer (CMA) (PHI Model 15-255 GAR) equipped with an internal coaxial electron gun and an angularly resolving movable aperture. ISS data were taken using a sputter ion gun (PHI Model 04-161) positioned at an angle of 60° with respect to the sample surface plane. The sample was positioned at an angle of 45° with respect to the CMA axis, and the angle resolving aperture was used to select He^+ ions scattered at an angle of 13° with respect to the sample plane for energy analysis. A primary beam of He^+ ions with an energy of 1 keV was used with the current to the sample being 0.6-0.74 μA over an area with an approximate diameter of 2 mm. LEED patterns were observed using a PHI Model 15-180 hemispherical grid system and a primary beam energy of 90 eV. TPD data were obtained using a quadrupole mass spectrometer (EAI Series Quad 250) by recording the intensity of the signals of as many as four masses simultaneously as a function of temperature.

Results and Discussion

Adsorption

ISS provides an excellent means of monitoring the amount of adsorbed species at a surface as a function of exposure. Due to the high surface sensitivity of ISS, the composition of the outermost one or two surface layers can be determined[104] if the scattering cross sections and ion neutralization probabilities are known.[105] The surface sensitivity of ISS is a result of the nearly 100% probability of neutralization or inealastic scattering for an ion which penetrates beneath the outermost layer of atoms. A potential problem with ISS is surface alteration due to sputtering. This was minimized in this study by using a relatively low primary beam flux and scanning over the N and Si peaks only. An ISS spectrum was taken over the entire range (E_1/E_0 of 0 to 1) preceeding the N_2 dosing to check surface cleanliness. Prior to N_2 dosing the ISS O signal was reduced to less than 5% of the Si peak height by IBA. This was the minimum O signal obtainable and is below the AES detection limit. In AES the noise level was typically less than 0.005 of the Si LVV (91 eV) peak intensity.

An ISS spectrum taken from a sample exposed to 75 L of N_2 at room temperature is shown in figure 3-1, and the ratio of N-to-Si ISS peak heights as a function of N_2 dose is shown in figure 3-2. The adsorption of N_2 on Si(111) under these conditions is characterized by an initial rapid linear uptake, a region of more gradual growth and saturation at approximately 75 L. A very important point is that

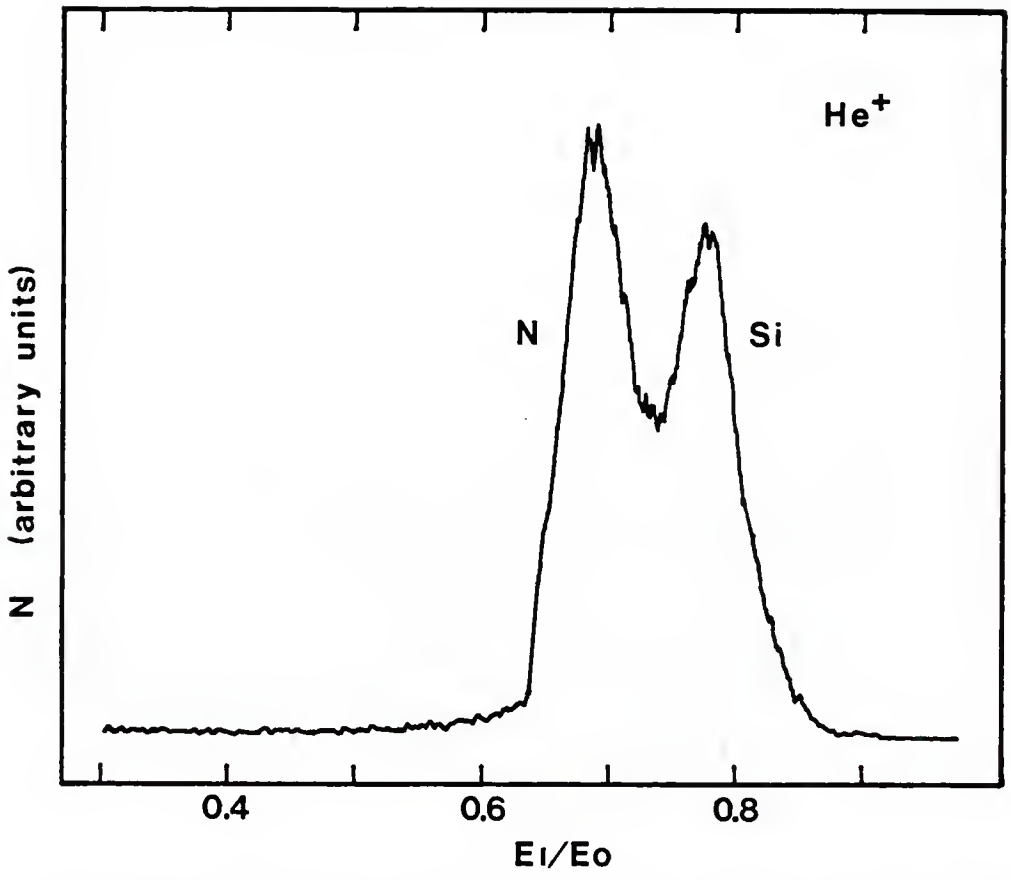

Figure 3-1. ISS spectrum taken from a Si(111) surface which had been exposed to 75 L of N_2 at room temperature. For a scattering angle of 73° E_1/E_0 is 0.70 for N and 0.79 for Si. All ISS data were taken at room temperature using 1 keV helium ions.

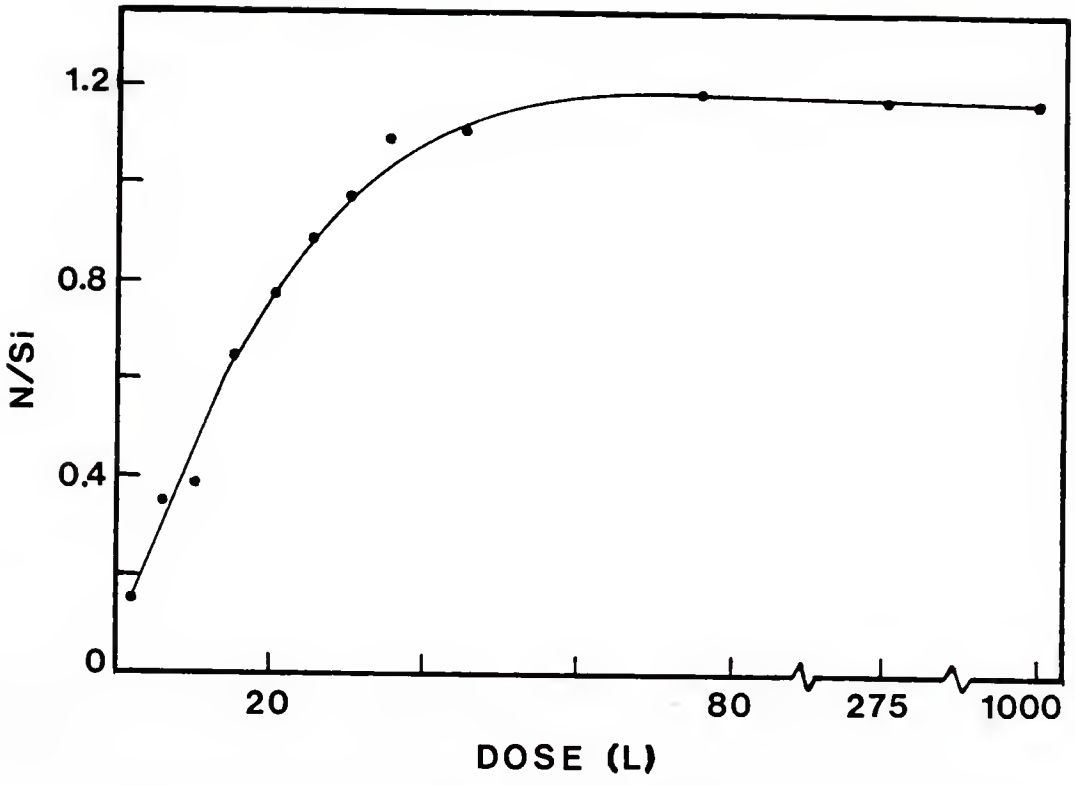

Figure 3-2. Ratio of N ISS peak heights to that of Si as a function of room temperature N_2 exposure.

at saturation coverage the amount of nitrogen present is below the detection limit of AES. This explains why Wiggins et al.[97] did not detect nitrogen adsorption using AES.

According to Parilis,[106] assuming a potential of the screened Coulomb Thomas-Fermi-Firsov form, a binary elastic collision and a primary ion beam energy of approximately 1 keV or higher, the differential cross section for scattering $(\frac{d\sigma(\theta)}{d\Omega})$ can be found from the expression:

$$\frac{d\sigma(\theta)}{d\Omega} = \frac{\pi^2(m_1 + m_2)a_o^{\,2}\, z_1 z_2 (13.68)(\pi - \Theta)}{m_2(z_1^{\,1/2} + z_2^{\,1/2})^{2/3} E_o (2\pi - \Theta)^2\, \theta^2 \sin\theta} \qquad (3\text{-}1)$$

$$\Theta = \theta + \arcsin(\sin\theta/\mu)$$

where the subscript 1 refers to the incident ion and 2 refers to the surface target atom, Z is the atomic number, $a_o = 0.468\ \mathring{A}$, $E_o(eV)$ is the primary beam energy, and Θ and θ are the scattering angles of the incident ion in center of mass and laboratory coordinates respectively. From equation (3-1) the differential scattering cross section, for $\theta = 73^\circ$, is 1.2×10^{-2} for Si and 6.2×10^{-3} for N. Then, the relative amounts of Si and N on the surface can be estimated from ISS peak heights assuming that the neutralization probabilities for He^+ scattering off N and Si are the same. At saturation the ratio of N-to-Si ISS peak heights is approximately 1.2 which yields a ratio of N-to-Si surface concentration of 2.2. This

implies that there are approximately 2 N atoms for each Si atom on the surface or approximately 2/3 of a monolayer of nitrogen on the Si(111) surface at saturation.

From the kinetic theory of gases, the rate of collision of N_2 with the Si sample surface at room temperature and a N_2 pressure of 10^{-7} Torr is 6.0×10^{13} collisions/sec. The sticking probability (s = rate of adsorption/rate of collision) can be found from the following expression:[107]

$$s(\bar{\theta}) = \frac{N_o}{\nu p} \frac{d\bar{\theta}}{dt} \qquad (3\text{-}2)$$

where $\bar{\theta}$ is the fractional coverage (number of molecules adsorbed/maximum uptake), N_o is the number of surface sites, ν is the number of molecules colliding with the surface (number/area·time) at room temperature, and p is the pressure. The initial sticking probability (s_o) can be obtained from the initial slope in figure 3-2 assuming $\bar{\theta}$ is 1 at saturation and the number of surface sites available for N_2 adsorption is half the number of surface Si atoms (= 1/2 (7.8×10^{14})).[107,108] In this study s_o is calculated to be 4.7×10^{-2}.

The LEED pattern was monitored throughout the room temperature N_2 adsorption steps. For doses up to saturation (75 L), a distinct (7x7) pattern remains. For much higher exposures (1000 - 3000 L), the (7x7) pattern deteriorates slightly (all spots become less sharply defined). These results are in agreement with the findings

of Heckingbottom.[95] The sample which had been exposed to 3000 L of N_2 at room temperature was then heated. The slightly deteriorated pattern remains unchanged for temperatures up to 570 °C. Upon heating to 670 °C the 1/7th order spots decrease in intensity relative to the (1x1) spots. This intensity change continues with further heating to 800 °C. The distinct (7x7) pattern is recovered by annealing the sample at 920 °C for 5 minutes. No features due to the (8x8) nor the quadruplet pattern were observed.

Desorption

TPD was performed in order to gain a better understanding of the adsorbed nitrogen. The experiments were carried out by exposing the sample to 1000 L of N_2 and then heating to approximately 770 °C. The amount of each desorption product (assumed to be proportional to the TPD peak area) varies with sample history. Nevertheless, considerable information can be extracted from the TPD data.

Desorption peaks occur at only two temperatures 320(T_1) and 510 °C(T_2). The masses of species which desorb at T_1 are 1, 2 and 14 amu. At T_2 masses of 1, 2, 14, 15, 16, 28 and 29 amu desorb. The TPD peaks have very distinct and repeatable shapes (see figure 3-3) which depend upon the kinetics of desorption.[109] The shape of the T_1 peak is indicative of first order kinetics while the shape of the T_2 peak probably suggests more complex desorption kinetics. Assuming that the rate of desorption can be described by an Arrhenius expression and that the desorption is first order, the relationship

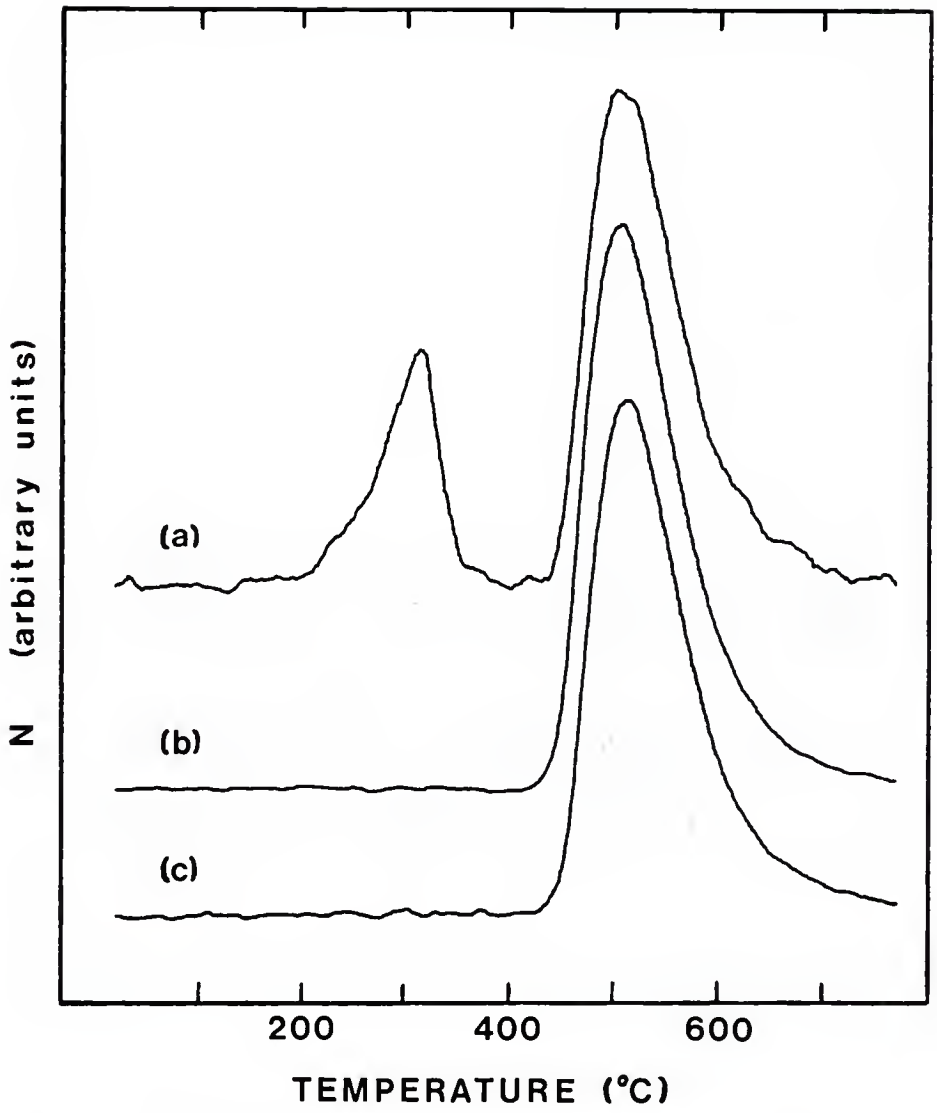

Figure 3-3. Typical TPD spectra for masses (a) 14, (b) 28 and (c) 29 for a sample which had been exposed to 1000 L of N_2 at room temperature. The ordinates of (a), (b) and (c) are not scaled relatively to one another. The experimental peak area ratios are $(a(T_1)):(a(T_2)):(b):(c) = 1:3.5:44.3:6.1$.

between the TPD peak temperature (T_p) and the desorption activation energy (E_d) is given as:[109]

$$\frac{E_d}{R\,T_p^2} = \frac{\nu}{\beta} \exp\left(\frac{-E_d}{R\,T_p}\right) \qquad (3\text{-}3)$$

where ν is the frequency factor (assumed to be 10^{13} sec.$^{-1}$) and β is dT/dt. Using this expression gives an $E_d(T_1)$ of 34.0 kcal/mol (1.5 eV/atom). This analysis probably does not apply to the T_2 peak since it probably is not first order.

The desorbing hydrogen is believed to come from the sample surface or near-surface region and is present prior to the adsorption of nitrogen. In fact, ESD has been used to verify the presence of hydrogen on the Si surface before and after exposure to nitrogen.[110] The hydrogen detected on the surface is not believed to be due to adsorption of background gases since attempts to adsorb D_2 at room temperature do not yeild TPD peaks for masses 3 or 4. Additionally, it is commonly believed that at room temperature molecular hydrogen does not adsorb appreciably on clean Si surfaces.[29,54] Therefore, it is most likely that hydrogen is present in the bulk of the Si and is not removed by the cleaning procedure. Furthermore, the concentration of surface hydrogen varies considerably with sample pretreatment and history.

In order to interpret the TPD results the cracking patterns due to the ionizer of the mass spectrometer and the isotope ratios must be taken into account.[111-113] These figures as well as average

experimental peak area ratios are given in table 3-1. With the aid of this table the TPD features are assigned as follows. The 28 amu peak is due to the desorption of N_2 and not Si for the following reasons: the experimental peak area ratio of the 28 and 29 amu peaks is not the same as the Si isotope ratio (see table 3-1); no peak is found for 30 amu corresponding to the 30 amu Si isotope; and most importantly, no desorption of masses 28, 29 or 30 is observed from a clean sample. The 29 amu peak is due to desorption of primarily N_2H since the ratio of the amount of 29 to 28 is too great for the 29 peak to be due mostly to desorption of $N^{14}N^{15}$ (see table 3-1). The 14 amu TPD peak is due to N desorption. The 15 amu peak is primarily due to NH desorption since the peak area ratio of 14 to 15 amu does not correspond with the ratio for the N isotopes (see table 3-1). The 16 amu peak is believed to be due to NH_2, and the 1 and 2 amu peaks are due to H and H_2, respectively. Species with masses greater than 29 amu are not observed. Fragmentation or cracking of N_xH_y species does occur in the ionizer, but the cracking patterns are not known for most of these species.

The majority of the atomic hydrogen detected is not due to the cracking of H_2 since for a number of trials H desorbs only at T_2 while H_2 desorbs only at T_1. At other times for the same dosing conditions but a slightly different sample history, H_2 desorbs at both temperatures (see figure 3-4). Factors which may affect the temperature at which H_2 desorbs as well as the TPD peak areas include the number of TPD runs done prior to the exposure to N_2 and

TABLE 3-1
Isotope, Cracking and Experimental TPD Area Information

	Isotope Ratios[a]		Average Experimental TPD Peak Area Ratios	
Species	mass(amu)	relative amount(%)	mass	relative amount(%)
Si:	28	92.21	14	80[d]
	29	4.70	15	7
	30	3.09	16	13
N:	14	99.63	28	78[e]
	15	0.37	29	22
			30	0
H:	1	99.985		
	2	0.015		
	Cracking Patterns[b,c]			
H_2:	1	2.6	14(T_1)	6[f]
	2	97.4	28(T_2)	94
N_2:	14	8.2	14(T_2)	8[g]
	28	91.15	28(T_2)	92
	29	0.65		
NH_3:	14	1.1		
	15	3.7		
	16	42.3		
	17	52.9		

Referenced relative amounts were converted to percentages. a) Reference 111, b) H_2 and N_2--reference 112, c) NH_3--reference 113, d) Taken from 1 TPD run, e) Ranged from 74-88% mass 28, f) Ranged from 92-98% mass 28, g) Ranged from 92-92.7% mass 28.

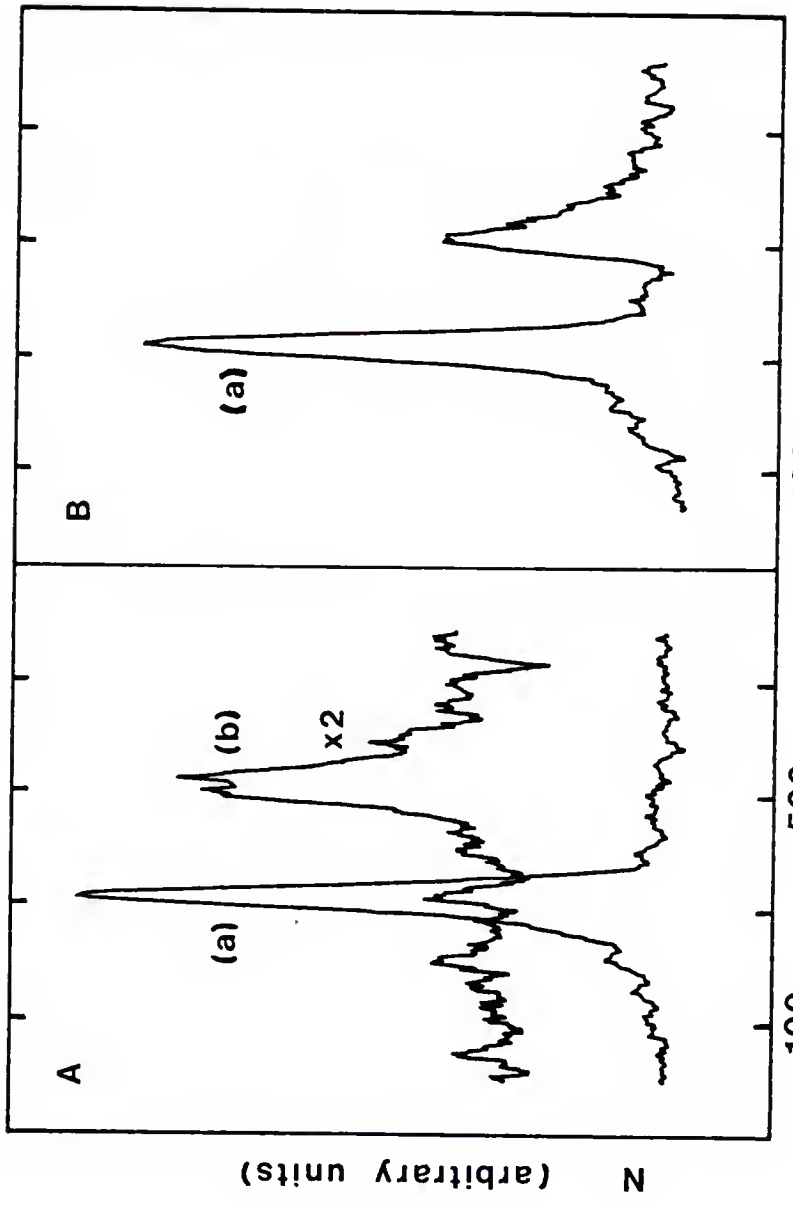

Figure 3-4. TPD spectra for a sample which had been exposed to 1000 L of N_2 at room temperature. Spectra labeled (a) refer to the desorption of H_2 and (b) refers to the desorption of H. The data in (A) were taken from a sample with a different history than the sample in (B) (see text).

subsequent TPD run, the heating and/or cooling rate for the 920 °C annealing step between doses and possibly the presence of nitrogen in the sample near-surface region following the annealing step. The hydrogen detected could be a result of the cracking of N_xH_y species. The facts that H and H_2 do not desorb at temperatures other than T_1 or T_2 and that their desorption peaks are the same shape as the nitrogen peaks suggest that hydrogen is associated with or bonded to the nitrogen on the surface.

TPD peak area comparisons reveal that the N desorbing at T_2 may be primarily due to the cracking of N_2 (which only desorbs at T_2) in the mass spectrometer (see table 3-1). It is possible that the NH and NH_2, which desorb only at T_2, are due to the cracking of N_xH_y species. The presence of relatively more N_2 on the surface than N_xH_y would explain the large amount of mass 14 detected with respect to the amounts of masses 15 and 16. Mass 17 was not detected, and considering the ratio of mass 15 to mass 16, it is not likely that any NH_3 desorbs (see table 3-1).

Following N_2 dosing and a thermal desorption experiment it is found using ISS that nitrogen remains on the Si surface. This may be due to nitrogen which is bound in a state which does not thermally desorb. In order to investigate the effects of the thermal desorption process on the adsorbed nitrogen, a series of repeated TPD runs were done without redosing between the runs. As the number of runs increase, there is a tendency for the TPD areas of species detected at T_2 to decrease while the areas of T_1 peaks either

slightly decrease or increase. This indicates that a portion of the species adsorbed in state 2 (T_2) may be populating state 1 (T_1) during TPD runs. For the case of hydrogen the analysis is not as straightforward. The complexity in the data suggests the coexistence of a number of competing processes which increase or decrease the amnount of hydrogen on the surface which is ultimately detected as H, H_2 or N_xH_y.

Conclusions

ISS and TPD have been used to study the interaction between N_2 and the Si(111)(7x7) surface. Using ISS, the adsorption of nitrogen as a function of dose was examined and a room temperature saturation dose of 75 L is found. Following a saturation dose nitrogen cannot be detected with AES. The initial sticking probability, s_o, of nitrogen on Si(111) is 4.7×10^{-2} at room temperature.

A distinct (7x7) LEED pattern remains for the surface exposed to 75 L of N_2 at room temperature. Additional exposures to N_2 and subsequent heating result in variations in this LEED pattern, but the distinct (7x7) pattern is recovered by annealing at 920 °C for 5 minutes. Features due to the (8x8) or the quadruplet pattern are not observed.

Using TPD, evidence of at least two chemisorbed states of nitrogen is found. These two states desorb at 320 and 510 °C with distinct and repeatable TPD peak shapes. Hydrogen also desorbs in the forms of H, H_2 and N_xH_y at the same temperatures and with the

same peak shapes as the desorbing nitrogen. This indicates that the hydrogen is associated with or bonded to the adsorbed nitrogen prior to thermal desorption. The hydrogen is believed to originate in the bulk of the Si sample.

CHAPTER IV
AN ELECTRON-STIMULATED DESORPTION STUDY OF THE INTERACTION OF HYDROGEN, DEUTERIUM AND OXYGEN WITH GaAs (100)

Introduction

The interaction between GaAs and hydrogen is an important topic which has been discussed in relatively few studies. Studies of this interaction may provide information which is useful in the growth of epitaxial films or passivating layers on semiconductor surfaces. It has been shown that atomic hydrogen introduced by hydrogen plasma exposure passivates certain electrically active deep-level defect sites[14,15] as well as certain shallow-level dopant sites[16] in GaAs. A similar effect is observed after incorporating hydrogen into GaAs electrochemically in a phosphoric acid electrolyte.[16] Reduction in electrical activity due to hydrogen passivation has been observed in silicon[2-4] and germanium[13] as well. Studies of this type are particularly important with regard to the growth of GaAs films using molecular beam epitaxy (MBE)[114] and chemical vapor deposition (CVD).[115-118] In the CVD process hydrogen is typically present either as a carrier gas[115] or in the compounds used to form the GaAs;[116-118] e.g. AsH_3 or $Ga(CH_3)_3$. It has also been shown that exposing GaAs surfaces to hydrogen plasmas provides an effective means of removing contamination.[119-121] For these reasons the role of hydrogen in the formation and preparation of GaAs and its effects on the properties of GaAs should be considered.

An early study by Pretzer and Hagstrum[122] used ion neutralization spectroscopy (INS) to study the (111), ($\overline{111}$) and (110) GaAs surfaces before and after a room temperature exposure to different gases including O_2, N_2, H_2 and CO. A 3×10^5 L exposure of a clean GaAs surface to H_2 causes no change in the INS spectrum. The authors conclude that molecular hydrogen does not adsorb at significant rates at room temperature on GaAs surfaces.

This finding was reaffirmed in the UV photoelectron spectroscopy (UPS) study of Gregory and Spicer[123] who investigated the adsorption of O_2, CO and H_2 on n- and p-type, single crystal, cleaved GaAs(110) surfaces. They found that atomic hydrogen readily adsorbs on p-type surfaces at room temperature causing a large change in the electron energy distribution curve (EDC) between 1.6 and 5.5 eV below the valence band maximum. For low exposures this adsorption is reversible in that heating the sample to about 235 °C results in an EDC which is quite similar to that of clean GaAs(110). By comparing these spectra with results of a study of Cs-covered GaAs (110),[124] Gregory and Spicer assert that adsorbed atomic hydrogen behaves like an alkali metal adsorbed on GaAs. Although room temperature adsorption of molecular hydrogen is not observed, a 3×10^7 L exposure to H_2 with the sample heated to about 415 °C results in adsorption. UPS shows that this adsorbed hydrogen is different than the atomically adsorbed hydrogen. Heating the sample to about 700 °C does not result in an EDC equivalent to an EDC from a clean surface. Gregory and Spicer suggest that a chemical compound may form or that hydrogen diffuses into the GaAs.

Mokwa et al.[125] used TPD to investigate the interaction between both molecular and atomic hydrogen and a cleaved GaAs(110) surface. They found no interaction between H_2 and the GaAs surface at 250 K. However, atomic hydrogen adsorbs readily. Heating causes desorption of AsH_3 at 340 K, H_2 at 450 K and Ga atoms above 700 K.

Lüth and Matz[126] used high resolution electron energy loss spectroscopy (HREELS) to study atomically adsorbed hydrogen and deuterium on both n- and p-type GaAs(110). They assigned loss features to H and D bonded to both Ga and As atoms and were able to construct Morse functions which adequately describe the electronic potential energy curves and a rate expression which describes thermal desorption of molecular hydrogen. Another HREELS study by Dubois and Schwartz[127] also identifies hydrogen atoms bonded to both Ga and As atoms on a (100) surface of chromium-doped GaAs. A lengthy anneal forms a Ga-rich surface, and the HREELS peak due to H bonded to As disappears. Electron energy loss spectroscopy (ELS) studies by Bartels et al.[128] and Mönch[129] found that hydrogen atoms initially bond to the As. Several studies[123,126,128,129] agree that a dipole or depletion layer forms at these surfaces upon adsorption of atomic hydrogen.

The polar (100) surface of GaAs is more complex than the (110) cleavage surface because it reconstructs in numerous ways resulting in a variable ratio of surface Ga-to-As atoms. The relationship between structure and composition has been examined[130,131] finding that the As coverage varies from about 0.27 to 1.00 as the surface

reconstructs with LEED patterns: (4x6), (1x6), c(8x2), c(2x8) and c(4x4). Bringans and Bachrach[132-135] have used angle-resolved UPS to study atomically adsorbed hydrogen on GaAs(100) and (111). They found that this surface always exhibits the same LEED pattern regardless of the original structure of the clean GaAs(100) and (111) surfaces before adsorption. The hydrided structure of GaAs(100) lies between the c(4x4) and c(2x8) structures, and annealing always yields the c(2x8) pattern. The GaAs($\overline{111}$) surface reverts to a (1x1) symmetry after a saturation exposure to hydrogen. The authors conclude that atomically adsorbed hydrogen on a GaAs(100) surface results in an As-rich surface which does not agree with the results of Dubois and Schwartz.[127] The UPS results show that adsorption of atomic hydrogen removes states from near the top of the valence band and introduces new states 4.3 to 5.2 eV lower. A surface state exists on this surface, and the fact that it does not disperse in the $\overline{\Gamma} \rightarrow \overline{K}$ direction suggests that it does not participate in bonding with the hydrogen.

Friedel and Gourrier[119] demonstrated that exposing a GaAs surface to a hydrogen plasma is an effective way to remove carbon and nitrogen contamination but is somewhat less effective for removing oxygen. Chang and Darack[120] have shown that a high frequency hydrogen plasma can easily etch GaAs at a rate of about 20Å/sec and that this rate is proportional to both the hydrogen pressure and the r.f. power of the discharge. A surface study of the effects of exposing a GaAs(001) surface to a hydrogen plasma has been reported

by Friedel et al.[121] In this study variations in the surface structure, high lying core levels of As and Ga and valence band were examined using angle-resolved UPS and reflective high energy electron diffraction (RHEED) as a function of exposure to the plasma. By curve resolving the As 3d and Ga 3d levels, they found that hydrogen induces a new peak on the Ga spectrum and possibly two on the As spectrum. They also believe that hydrogen initially bonds to the As atoms and then to the Ga atoms at higher exposures. The Ga-to-As ratio increases with plasma exposure, and the surface becomes more disordered.

Many surface techniques including XPS, UPS, ELS and ISS are relatively insensitive to hydrogen or can observe hydrogen only indirectly through its influences on other spectral features. This is usually due to its small cross section, light mass or lack of core-level electrons. HREELS is an example of a technique in which features due specifically to hydrogen are observed. Techniques which rely upon a mass spectrometric determination of hydrogen are also directly sensitive to hydrogen. This has been demonstrated in an early study by Madey and Yates[136] in which they found ESD of H^+ from a cleaved, p-type GaAs(110) surface. H^+ desorbs from both the freshly cleaved surface and from a cesiated surface. They attributed the presence of this hydrogen to adsorption of background hydrogen. In the present study the usefulness of ESD in studying the interaction of hydrogen with GaAs(100) and oxidized GaAs(100) was investigated. This represents an initial attempt to use ESD to

examine hydrogen on GaAs surfaces in which the following questions are considered. Under what conditions does hydrogen adsorb on GaAs surfaces? Can ESD provide a measure of the amount of adsorbed hydrogen? Is it possible to distinguish between different adsorbed states of hydrogen using ESD? The preliminary results presented here demonstrate that ESD is a useful technique for studying the interaction of hydrogen with GaAs and, most probably, with other III-V materials.

Experimental

A cut and polished, undoped single-crystal GaAs sample furnished by MACOM was used in this study. It was produced using the liquid-encapsulated Czochralski crystal growth method. A room temperature chemical etch with a weak sodium hypochlorite solution was used to produce a mirror finish of the (100) surface (±2°). After solvent cleaning the sample in an ultrasonic bath of electronic grade trichloroethylene followed by acetone and then methanol, the sample (10 x 16 x 0.5 mm) was mechanically supported by a copper holder. A 0.5 mm diameter tungsten filament was mounted behind the sample for radiant heating. The temperature of the sample was measured using an iron-constantan thermocouple, which was mechanically pressed against the sample, and an optical pyrometer was used over the range of 230 to 560 °C. After inserting the sample, the vacuum system was baked for 24 hours at 200 °C and pumped down to a base pressure of 2×10^{-10} Torr. The sample was cleaned using cycles of room temperature,

argon ion bombardment followed by annealing (IBA). Specific conditions used were an Ar ion sputter at a beam energy of 1.0 keV and a beam current of 1 μA over an area of approximately 2 mm in diameter for 15 minutes, a 5 minute anneal at 500 °C, an Ar ion sputter at a beam energy of 1.0 keV and a current of 1.5 μA for 30 minutes concluding with a 500 °C anneal for 5 minutes. This procedure results in a clean surface as determined by AES. AES spectra taken from the contaminated and clean sample are shown in figure 4-1, curves (a) and (b), respectively.

The vacuum system used in these experiments has been described previously.[1] AES and ESD were performed using a double-pass cylindrical mirror analyzer (CMA)(PHI Model 15-255 GAR) equipped with an internal coaxial electron gun and an angularly resolving movable aperture. AES spectra were taken in the nonretarding mode using an oscillation of 10 kHz and 0.5 V peak-to-peak, a primary beam energy of 3 keV and a current of 25 μA over a spot size of approximately 0.1 mm in diameter.

ESD data were taken using the CMA as a time-of-flight mass spectrometer as discussed by Traum and Woodruff.[69] Electronic control and data collection were performed using a PDP 11/02 computer system and a computer-interfaced digital pulse counting circuit developed by Gilbert et al.[137] In these experiments energy analysis of low energy (less than 20 eV) positive ions was accomplished by operating the CMA in the retarding mode with a pass energy of 80 eV. The ions were first accelerated by a negative potential placed

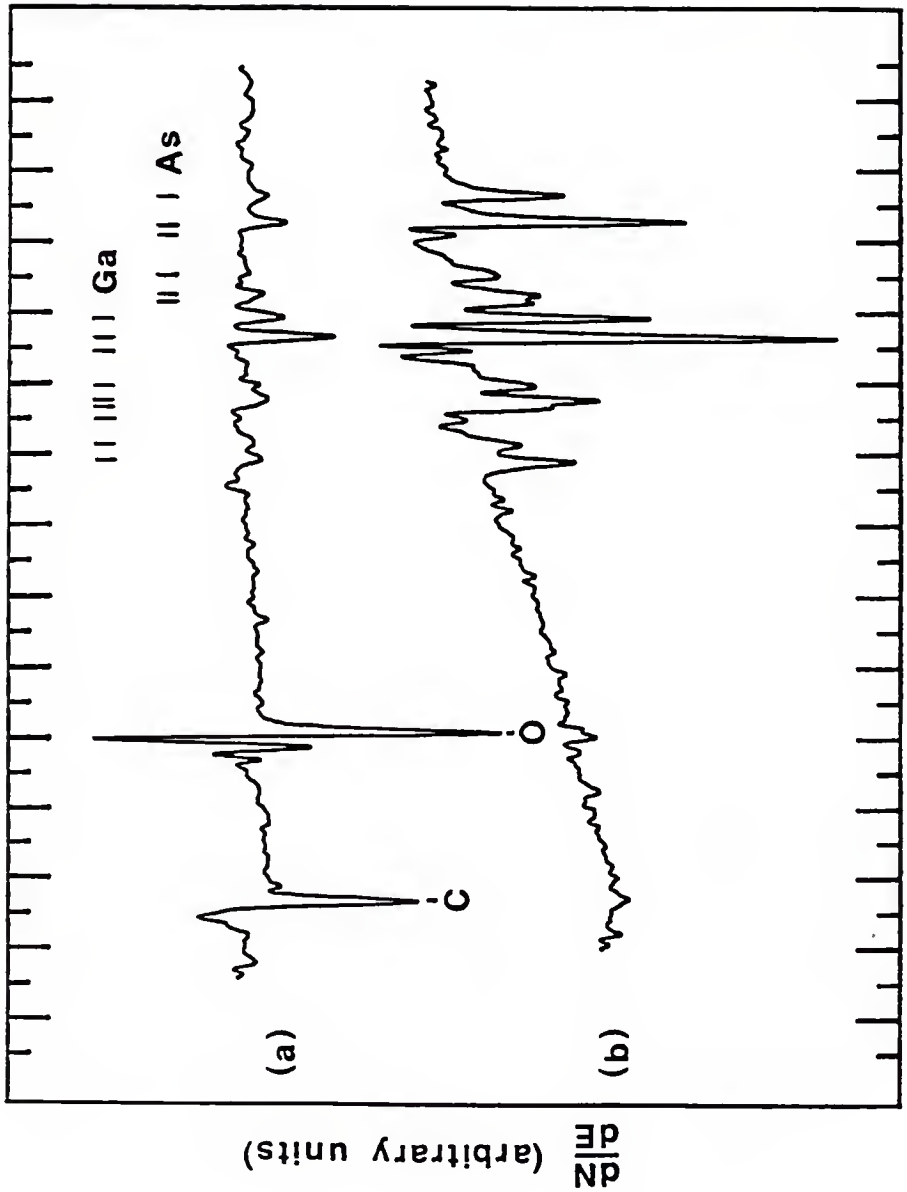

Figure 4-1. AES spectrum (a) of contaminated GaAs(100) taken after solvent cleaning and (b) taken after the IBA cleaning procedure.

on the second grid and inner cylinder. The outer cylinder was maintained at a more positive potential (but negative potential with respect to ground) than the inner cylinder. The complete set of operating voltages has been published previously.[70] For mass analysis the electron beam was pulsed onto the sample for 300 ns using the electron gun deflector plates in the CMA. After an appropriate delay period (4.2 μs for H^+, 5.8 μs for D^+ or 16.8μs for O^+) pulses were counted for a 300 ns period. A primary beam energy of 140 eV and primary beam current of about 500 nA were used. The sample was biased at +10.0 V. It was mounted at an angle of 45° with respect to the electron beam, and ions desorbing in the direction normal to the sample were selected with the movable aperture.

Three different types of ESD spectra were taken in this study. A mass spectrum of the desorbing ions was obtained by selecting an ion kinetic energy and scanning the delay time. An ESDIED spectrum was obtained by selecting a delay time appropriate to the ion of interest and scanning the kinetic energy with the CMA. The total-ion energy distribution was obtained by scanning ion kinetic energy without time gating.

Results and Discussion

In ESD electrons impact a surface creating localized excitations which can decay causing desorption of ions, neutrals and metastable species. Thus ESD is a destructive process in that it alters the composition and structure of the surface. Beam exposures were

minimized in these experiments to reduce surface damage while still obtaining acceptable signal-to-noise ratios. In many cases a second spectrum was taken, and since in each case this duplicates the initial spectrum, it is assumed that effects due to beam damage are negligible.

ESD is a complicated technique in that it can be performed in many different ways to obtain various types of information about bonding at a surface and/or the mechanism of excitation and desorption. These topics have been discussed in a recent review article[70] and are only considered when they are directly related to the results presented here. Several points regarding ESD which do relate to this study are its surface sensitivity, the isotope effect and cross section determination.

In ESD a low energy ion can desorb only from the top monolayer. Ions which are created below the top monolayer have a nearly 100% probability of being neutralized during the desorption process. However, excitations created beneath the surface can emit secondary electrons which can create excitations at the surface causing emission of ions.[71] Thus, ESD is highly surface sensitive (outermost monolayer) with respect to the emitted ionic signal but not so surface specific with respect to the primary electron beam.

The ESD mass spectrum shown in figure 4-2 was taken from the contaminated surface corresponding to figure 4-1(a). The peak at 4.2 μs reveals the presence of hydrogen, but ESD peaks due to positive ions containing carbon or oxygen do not appear although the surface

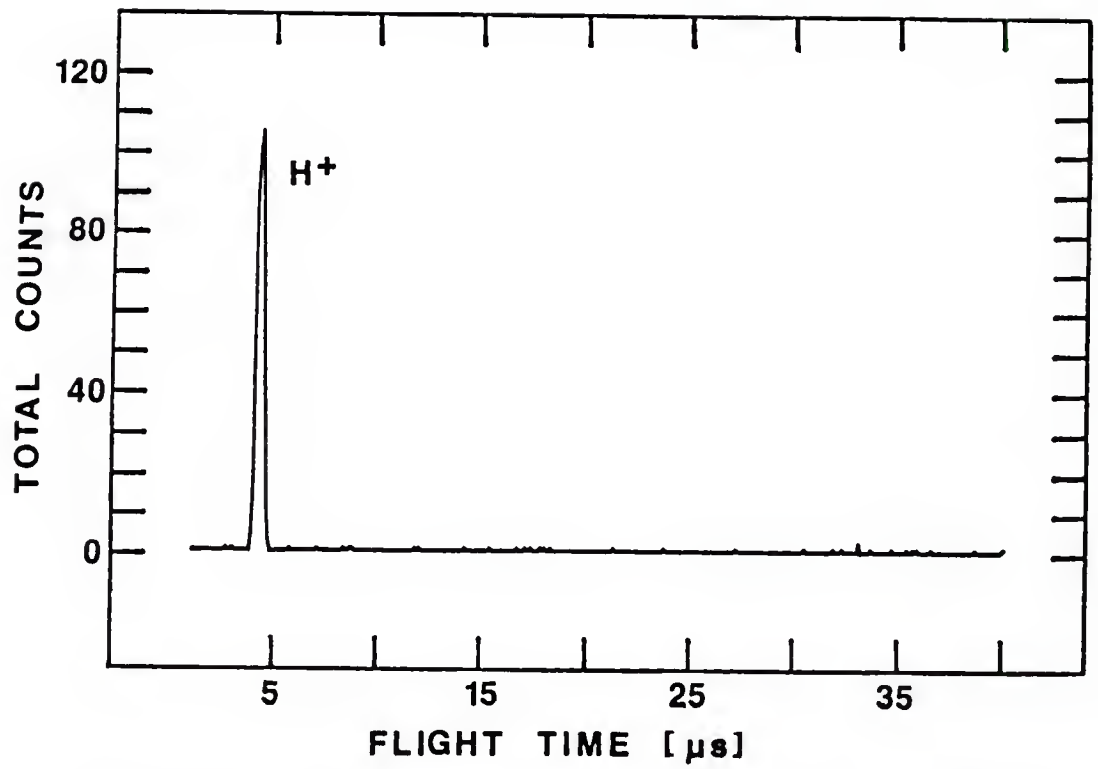

Figure 4-2. ESD mass spectrum taken from the contaminated surface corresponding to figure 4-1(a). All ESD spectra were taken using a primary beam energy of 140 eV.

is heavily contaminated with these species. After IBA cleaning the ESD mass spectrum appears the same except that the total count due to H^+ is reduced by a factor of 8 using the same data collection parameters. This indicates that hydrogen is present as a surface species even on a "clean" GaAs surface. Drawing an analogy between GaAs and Si, which readily chemisorbs hydrogen and forms a hydride[2-4,72] may be useful in understanding the interaction between hydrogen and GaAs. GaAs is both isoelectronic and isostructural with Si except GaAs has a slightly larger lattice constant and its bonding structure is less covalent. These facts suggest that a hydride compound of GaAs may form and support the supposition of Gregory and Spicer[123] that hydrogen diffuses into GaAs forming a compound.

The surface concentration of hydrogen present in these experiments is not known. In order to determine the surface concentration of hydrogen using ESD, it is necessary to know the total cross section for desorption. ESD cross sections of adsorbed species vary over a large range but generally are orders of magnitude smaller than the corresponding gas phase cross section due to the high reneutralization probability of the escaping ions. However, an independent measurement of the surface concentration is required to determine the ESD cross section. As pointed out above, this is difficult with hydrogen. An attempt was made to use TPD to estimate the amount of hydrogen and deuterium present, but the sample mount was too massive to perform high-quality TPD. A very crude estimate from the TPD results suggests that tenths of a monolayer of deuterium

are adsorbed during the dosing procedure used. Efforts are being made to improve the quantification of these results.

Regardless of the cleaning procedure used, hydrogen is always present on the surface. It is possible that the surface hydrogen originally present is not completely removed, that the surface adsorbs background hydrogen during the cleaning process or that hydrogen in the bulk diffuses to the surface during annealing. In order to distinguish between surface hydrogen which is always present and hydrogen which is adsorbed under particular conditions, deuterium was used in these experiments. It was verified that molecular deuterium does not adsorb on GaAs at significant rates at room temperature. Heating the sample radiantly is known to dissociate D_2 which effuses to the surface even when the filament is not in line-of-sight of the surface.[134] It is assumed in these studies that the adsorbed deuterium is due to adsorption of dissociated deuterium but the adsorption of some molecular deuterium cannot be ruled out. The dose rate of deuterium atoms in these studies is only known in a relative sense.

Figure 4-3 shows an ESD mass spectrum taken after exposing the clean surface to a 2000 L dose of D_2 while maintaining the sample at 200 °C. In addition to the H^+ peak, which is the typical height from a clean surface, a peak due to D^+ appears at a flight time of 5.8 μs. Determining the relative amounts of adsorbed hydrogen and deuterium from this data is not straightforward because ESD exhibits an isotope effect which is particularly large for hydrogen. The

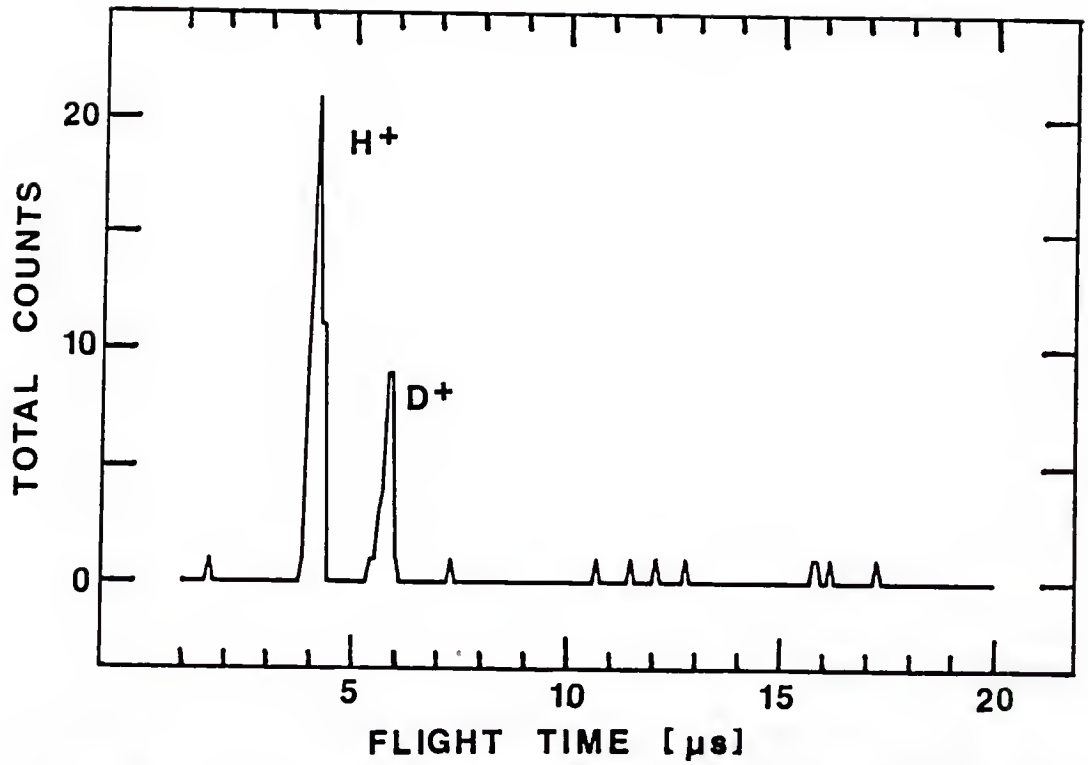

Figure 4-3. ESD mass spectrum taken after exposing the clean GaAs surface corresponding to figure 4-1(b) to a dose of 2000 L of D_2 while heating the sample at 200 °C.

desorption cross section is proportional to exp ($-c\sqrt{M}$) where c is a constant and M is the mass of the desorbing ion.[138] An isotopic ion of higher mass leaves the surface with approximately the same kinetic energy as a lower mass isotopic ion. Thus, the heavier ion desorbs with a lower velocity and has a greater probability for reneutralization. This has been verified experimentally. The ratio of the ionic desorption cross sections for H^+ and D^+ desorbing from a tungsten surface is greater than 100:1.[139-141] By this reasoning figure 4-3 suggests that the surface concentration of deuterium is greater than the surface concentration of hydrogen by a factor of approximately 50.

The total-ion energy spectrum and ESDIED spectra of H^+ and D^+ are shown in figures 4-4(a), (b) and (c), respectively. Due to the similarities of figures 4-4(b) and (c), it is believed that hydrogen and deuterium are desorbing from the same adsorbed state by the same mechanism. Unfortunately, it is not known if hydrogen desorbs from states bound to Ga or As atoms or both. The spectra were taken in the order (c), (b), (a). Comparing the high energy tails of these spectra suggests that with increased exposure to the primary beam, a higher kinetic energy state may appear or that hydrogen is initially present in another state. This is seen most readily by comparing the widths of the H^+ and D^+ spectra with the width of the total-ion spectrum. This second state would have a lower desorption cross section than the more prominent state or it would be less densely populated and, therefore, would require a larger beam exposure to build up a significant count.

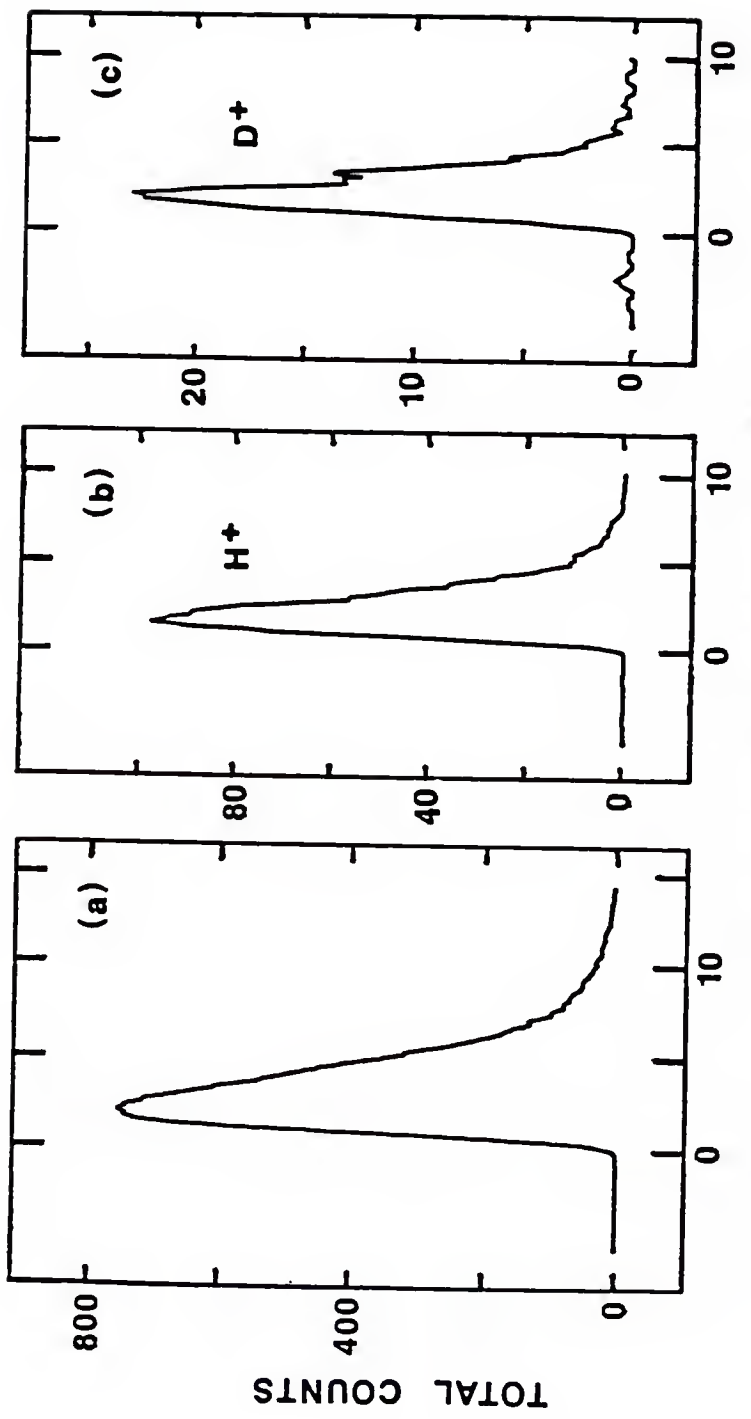

Figure 4-4. ESD spectra corresponding to the mass spectrum shown in figure 4-3. (a) Total-ion (H^+ and D^+) energy distribution spectrum and ESDIED spectra of (b) H^+ and (c) D^+.

Following the 2,000 L D_2 dose at 200 °C, the sample was heated to 500 °C for 10 minutes. ESDIED spectra taken before and after heating are quite similar in shape. However, after heating the D^+ signal of the ESD mass spectrum is reduced by a factor of 2 with respect to the H^+ signal which essentially remains unchanged. This result agrees with the results of Gregory and Spicer[123] in which adsorbed hydrogen could not be totally removed from the surface after a 3 x 10^7 L exposure to molecular hydrogen with the sample heated at 415 °C. As stated above, it is possible that both molecular and atomic deuterium adsorb during dosing at elevated temperatures in this study. It was also found that dosing the sample at 400 °C rather than 200 °C results in spectra identical to those shown in figures 4-3 and 4-4.

In order to examine the influence of surface oxygen on the interaction between hydrogen and GaAs, the clean surface was oxidized by dosing with 12,000 L of O_2 at room temperature. The resulting AES spectrum is shown in figure 4-5. Again, an ESD mass spectrum taken after a 2,000 L dose of D_2 at room temperature shows no evidence of deuterium adsorption. However, heating the sample above 200 °C while dosing causes adsorption of deuterium. The H^+ and D^+ counts are about 50% greater from the oxidized surface than from the clean surface, and the ratio of D^+ to H^+ is similar for both surfaces. It was also found that deuterium adsorbs more readily on a freshly oxidized surface than on a vacuum-aged (1 week at 10^{-10} Torr) oxidized surface. The normalized H^+ count from a vacuum-aged surface

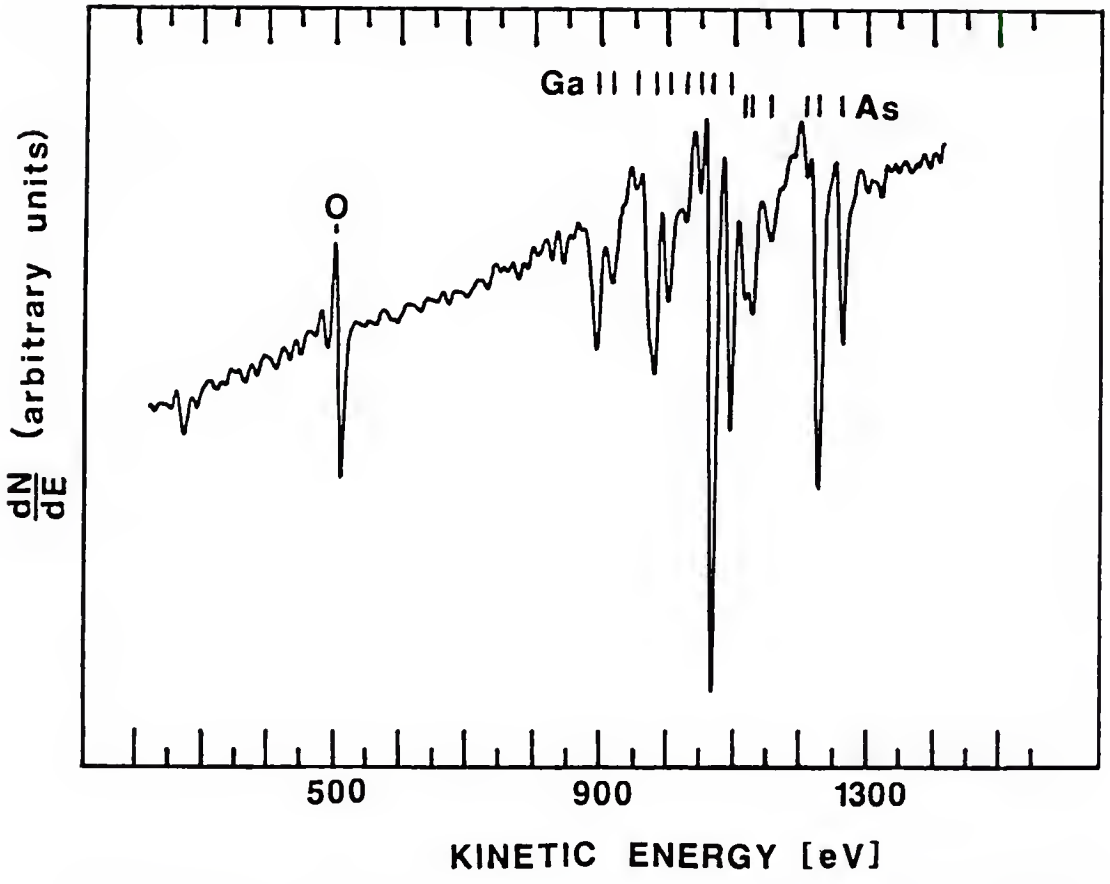

Figure 4-5. AES spectrum taken from GaAs(100) after a dose of 12,000 L of O_2 at room temperature.

is 3 times as large as the count from a freshly oxidized surface. Possible explanations for this behavior are that an oxidized surface adsorbs water molecules during a long exposure to the background gas in the UHV system or that the ion gauge tube filament dissociates background hydrogen which then adsorbs at the surface.

ESDIED spectra of the oxidized surface after exposure to 2,000 L of D_2 while heating the surface at 200 °C are shown in figure 4-6. The total-ion energy spectrum shown in figure 4-6(a) clearly reveals the presence of a high kinetic energy shoulder. The presence of two states is exibited by figures 4-6(b) and (c) for H^+ and D^+ respectively. However, the relative ratios of ions from the two states are different for hydrogen and deuterium, and the ratios vary as a function of beam exposure time. ESD mass spectra taken at ion kinetic energies of 0.8 and 3.55 eV are shown in figures 4-7(a) and (b) respectively. This figure shows that the deuterium-to-hydrogen ratio is a function of ion kinetic energy. The difference in concentration ratios is consistent with the interpretation that at least two different binding states of hydrogen are present. The precise nature of these states remains to be investigated.

Vasquez et al.[142] have suggested that hydroxyl groups on GaAs surfaces decompose according to the reaction

$$2Ga(OH)_3 \rightarrow Ga_2O_3 + 3H_2O \qquad (4\text{-}1)$$

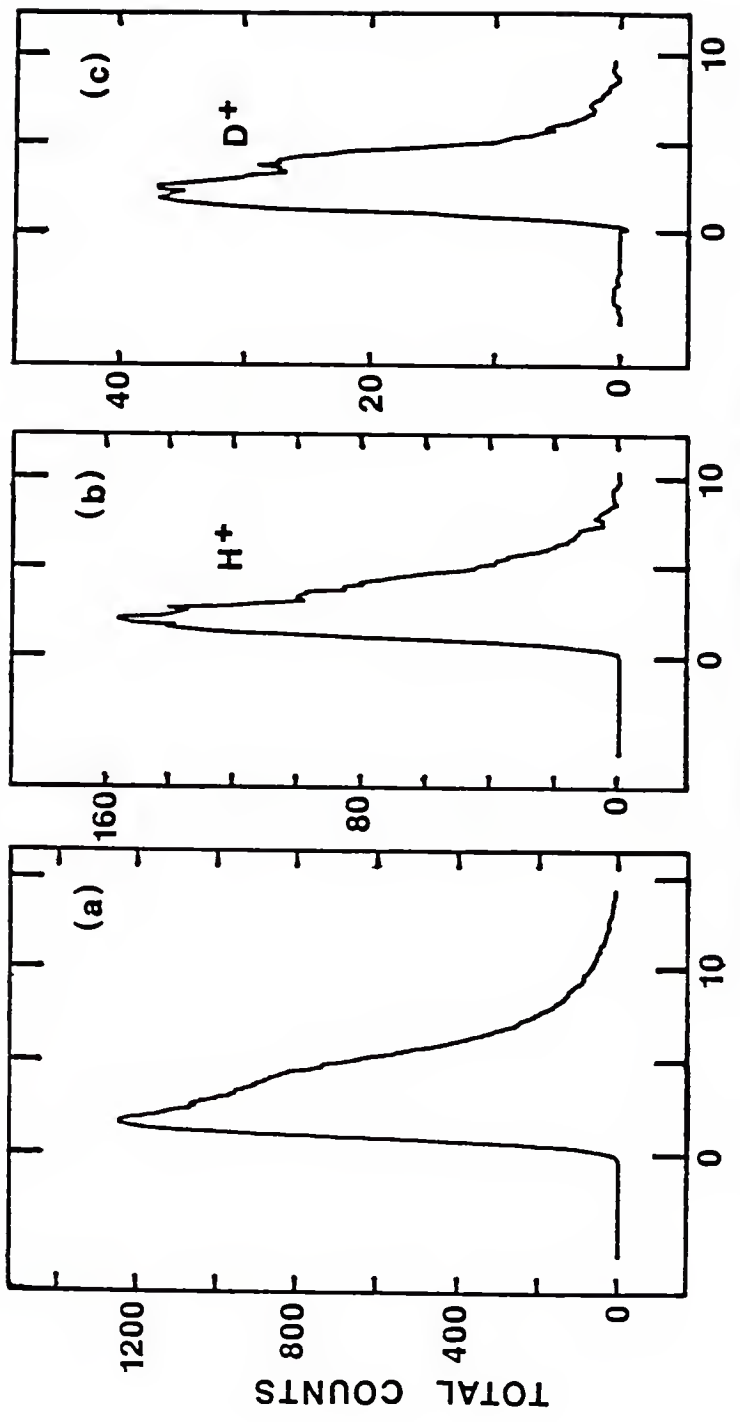

Figure 4-6. ESD spectra taken after exposing the oxidized surface corresponding to figure 4-5 to 2000 L of D_2 while heating the sample at 200 °C. (a) Total-ion (H^+ and D^+) energy distribution spectrum and ESDIED spectra of (b) H^+ and (c) D^+.

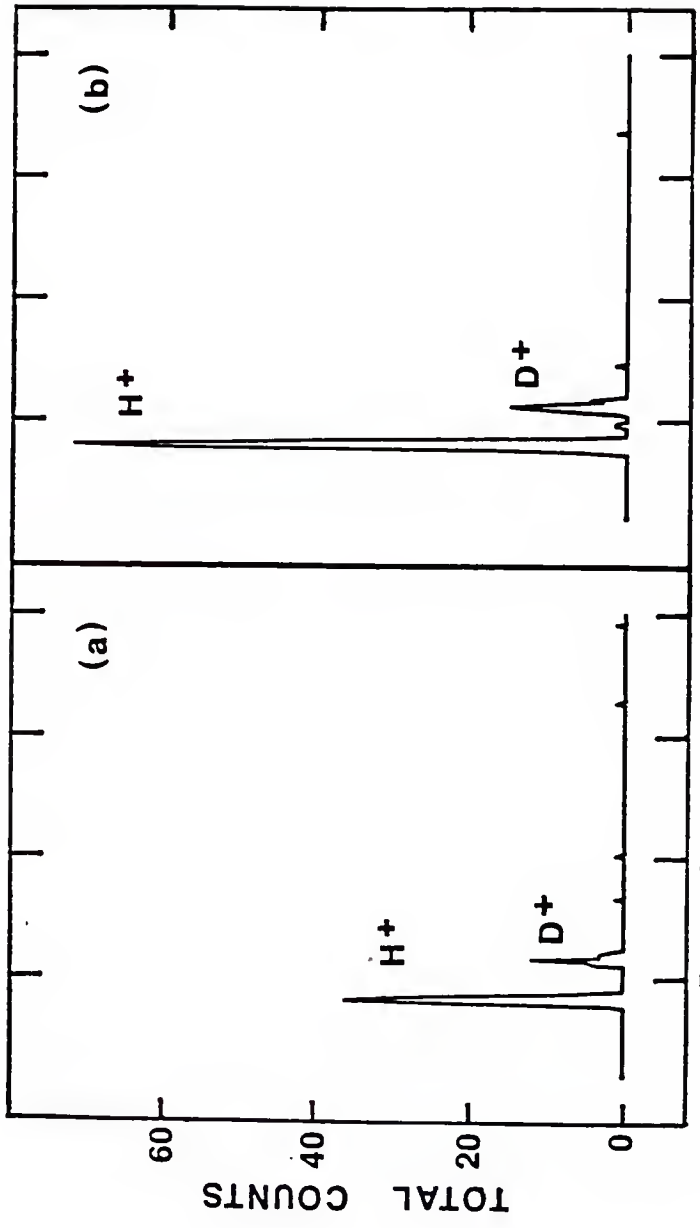

Figure 4-7. ESD mass spectra taken (a) at an ion kinetic energy of 0.8 eV and (b) at an ion kinetic energy of 3.5 eV.

at elevated temperature thereby reducing the oxygen content in the surface region. This was considered in this study. It was found that heating the deuterated, oxidized surface to 500 °C results in a very large decrease in the ESD D^+ signal. Also, monitoring the desorbing species with a quadrupole mass spectrometer while increasing the sample temperature shows that D_2, HD and H_2 desorb and that no H_2O or other oxygen-containing species desorb. If hydroxyl groups form under the dosing conditions used in this study, then heating causes them to form molecular hydrogen leaving the oxygen on the surface. This observation is also consistent with the fact that surface oxygen on GaAs is more resistant to removal by a hydrogen plasma[119] than other contaminants.

Conclusions

AES and ESD have been used to study the interaction between deuterium and both clean and oxidized GaAs(100). Cleaning was performed using IBA cycles, but it is not possible to remove the surface hydrogen completely. Molecular deuterium does not adsorb on either surface at significant rates at room temperature, but heating the samples radiantly between 200 and 400 °C with a hot filament causes adsorption of deuterium. A partially successful attempt to use TPD to quantify the amounts of adsorbed deuterium indicates that a few tenths of a monolayer probably adsorb during the dosing period. Taking the ESD isotope effect into account, it is estimated that the amount of adsorbed deuterium is about 50 times the amount of

residual hydrogen. Energy analysis of the desorbing ions indicates that at least one and possibly two adsorbed states are present on the clean GaAs(100) surface, but the nature of the adsorption states is not known. Heating the sample at 500 °C reduces the amount of adsorbed deuterium. It is presumed that most desorbs, but some may diffuse into the bulk.

The ESD H^+ and D^+ signals from the oxidized surface are about 50% greater than those from the clean surface after dosing under the same conditions. ESDIED clearly demonstrates that at least two adsorption states of hydrogen are present on the oxidized surface. Heating the sample to 500 °C causes desorption of D_2, HD and H_2, but no oxygen or oxygen-containing species desorb from the deuterium-dosed, oxidized GaAs(100) surface.

Although much remains to be done in characterizing the interaction of hydrogen with GaAs surfaces, and more generally with III-V semiconductor surfaces, the results presented in this chapter demonstrate that ESD provides a very useful technique for this type of study. It is now important to quantify the ESD results more accurately and to characterize the adsorbed states of hydrogen. Both are possible through the combined use of other surface techniques with ESD.

CHAPTER V
A CHARACTERIZATION STUDY OF THE NATIVE OXIDE LAYER FORMED ON CHEMICALLY ETCHED InP(111)

Introduction

InP is becoming an important III-V semiconductor material for fabrication of semiconductor devices.[20-23] Small changes in the composition of InP surfaces can significantly influence the electronic structure at the surface.[143] Thus, the properties of epitaxial layers and, consequently, of the final devices are determined by the surface of the InP substrate and any oxide layer which may be present. For this reason it is important to characterize native oxide layers on InP substrates. Often the native oxide layer is completely removed by polishing procedures or is partially removed during chemical etching steps. Characterization of the additional oxide formed upon exposure to air or formed by various methods of oxidation is also important.

Numerous studies of the oxidation of InP have been performed in order to investigate the growth mechanisms, surface compositions and oxidation states of the surface species using various methods of oxidation such as thermal oxidation,[144,145] high-pressure thermal oxidation,[146] photoenhanced thermal oxidation,[147] photoenhanced oxidation,[148] chemical oxidation[149] and electron-stimulated oxidation.[150] The effects of etchants on InP surfaces and oxide layers have also been investigated[151-154] as have the effects of sputtering,[155-157] annealing[158-160] and exposure to vacuum.[143,161]

XPS, SIMS and X-ray diffraction were used by Nelson et al.[144] to study the thermal oxides of p-type InP(100) formed in ~1/3 atm of O_2. They suggest that for a temperature in the range of 400 to 600 °C an outer layer of In_2O_3 and $InPO_4$ is formed and an inner layer of primarily $InPO_4$ is formed. Elemental P is observed at the oxide/bulk interface. For T>650 °C the oxide is composed of $InPO_4$. Yamaguchi and Ando[145] report that a polycrystalline oxide composed of $InPO_4$ (In_2O_3+P_2O_5) forms during a thermal oxidation (450-500 °C) of an undoped InP(100) surface in dry oxygen (0.2-2 atm). At higher temperatures the oxide is mostly In_2O_3. Infrared absorption and electron diffraction data suggest that for T>620 °C the oxides become In rich and lower oxides (possibly In_2O) form due to the loss of phosphorous. Wilmsen et al.[146] find that bulk oxides consisting of $InPO_4$, In_2O_3 and P_2O_5 form at elevated temperature (450 °C) and high oxygen pressures (42-500 atm). Faithpour et al.[147] used XPS and SEM to investigate the laser-enhanced thermal oxidation of n-type, semi-insulating InP(100) in a N_2O atmosphere. They found that In_2O_3 and a phosphate species form and that the growth rate is a function of the light intensity, N_2O pressure and temperature. The phosphate layer thickness is believe to be limited by the outwardly diffusion of phosphorus, which has also been suggested by Nelson et al.[144] The photon-stimulated oxidation of cleaved InP(110) studied by Koenders et al.[148] results in the formation of a depletion layer, but the fact that no surface dipole is introduced suggests that oxygen is incorporated into the lattice rather than adsorbed at the surface.

Exposure to oxygen with and without photon stimulation results in depletion of phosphorus at the surface in addition to formation of indium oxide. The chemical oxidation of n-type InP(100) in hot nitric acid also reveals a depletion of surface phosphorus as discussed by Korotchenkov et al.[149] Annealing and exposure to vacuum increases the amount of phosphorus in the surface region. Electron-stimulated oxidation of n-type InP(100) was investigated by Oliver et al.[150] using AES, LEED and ELS. In_2O_3 and a volatile phosphorus oxide form in the electron irradiated region. Heating above 500 °C causes the formation of small droplets of elemental indium. Clark et al.[151] used angle-resolved XPS to investigate the oxide layers and hydrocarbon contamination of InP surfaces after numerous treatments. The as-received samples were found to be phosphorus rich, but various treatments result in substantial differences in the composition of the surface region. Bertrand[153] concludes that the use of different etchants causes the amount of oxidized phosphorus on n-type InP(100) surfaces to vary. However, significant amounts of oxidized indium were found only on a sample which was heavily oxidized in air. Oxides formed in air after chemical etching with Br-MeOH were studied by Wager et al.[152] The as-etched surface is only slightly oxidized and is primarily a phosphorus oxide.

Thus far, most of the InP studies have focused on the (100) and (110) surfaces with only a few studies of the (111) surface.[145,154,162,163] This may be due to the difficulties encountered in obtaining a mirror finish using conventional etching

procedures.[154] In this study angle-resolved XPS, AES and ISS are used to examine the oxide layer formed on chemically etched InP(111) by exposure to air.

Experimental

An undoped InP(111) face cut to ±1° was furnished by Sumitomo Electric Industries, Ltd. for this study. The sample was grown by the liquid encapsulated Czochralski method and was polished using a mixture of ZrO_2 and NaOCl and then a mixture of SiO_2 and NaOH. The sample was then etched with H_3PO_4:HBr (2:1) to produce a mirror finish. The electrical properties and etch pit density are: carrier concentration $\leq 10^{16} cm^{-3}$ (n type), resistivity at room temperature = 1.8-1.9 x 10^{-1} ohm-cm, mobility = 3.9-4.0 x 10^3 $cm^2V^{-1} \cdot s^{-1}$ and E.P.D. $\leq 10^5 cm^{-2}$. The as-received sample was cut using a wafer saw to 21 x 15 x 0.35 mm and was ultrasonically cleaned for 5 minutes in each of the following electronic-grade solvents: trichloroethylene, acetone, methanol and then rinsed in deionized water.

A Perkin-Elmer PHI model 570 analytical system with a base pressure of 2 x 10^{-10} Torr was used in this study. The data was collected at Perkin-Elmer Physical Electronics in Eden Prairie, MN. A double-pass cylindrical mirror analyzer (CMA) with an internal electron gun and angularly resolving movable aperture was used to collect AES, XPS and ISS data. AES spectra were taken using a primary beam energy of 5 keV and a beam current of 0.3 μA rastered over an area of 2 x 2 mm. XPS spectra were taken using a Mg anode at

a voltage of 14 kV and power of 300 watts. High resolution XPS spectra were obtained using a pass energy of 25 eV which resulted in a total energy resolution of 0.75 eV. The high resolution XPS spectra were taken in the angle-integrated mode and angle-resolved mode at take-off angles of 10° and 85° with respect to the surface plane. ISS spectra were obtained using a 1 keV beam of $^{3}He^{+}$, a scattering angle of 144° and the movable aperture for improved resolution. For all spectra taken, the sample was placed at an angle of 50° with respect to the CMA normal.

In this study nondestructive techniques were used before destructive techniques. Thus, the techniques were used in the following order: XPS, angle-resolved XPS, AES, ISS and depth profiling using argon-ion sputtering. The results are not presented in this order in the following section.

Results and Discussion

Figure 5-1 shows the ISS spectrum taken from the air-exposed InP(111) surface. Three peaks are discerned corresponding to In, P and O, and the In peak is much larger than the other two peaks. ISS is essentially outermost layer sensitive for two reasons. The first is that ions which penetrate beneath the top layer have a very high probability of being neutralized, and the second is that even if they are not neutralized, they usually scatter inelastically during escape from the solid. In either case ions scattering off subsurface atoms do not contribute to the ISS peaks. Inelastically scattered ions

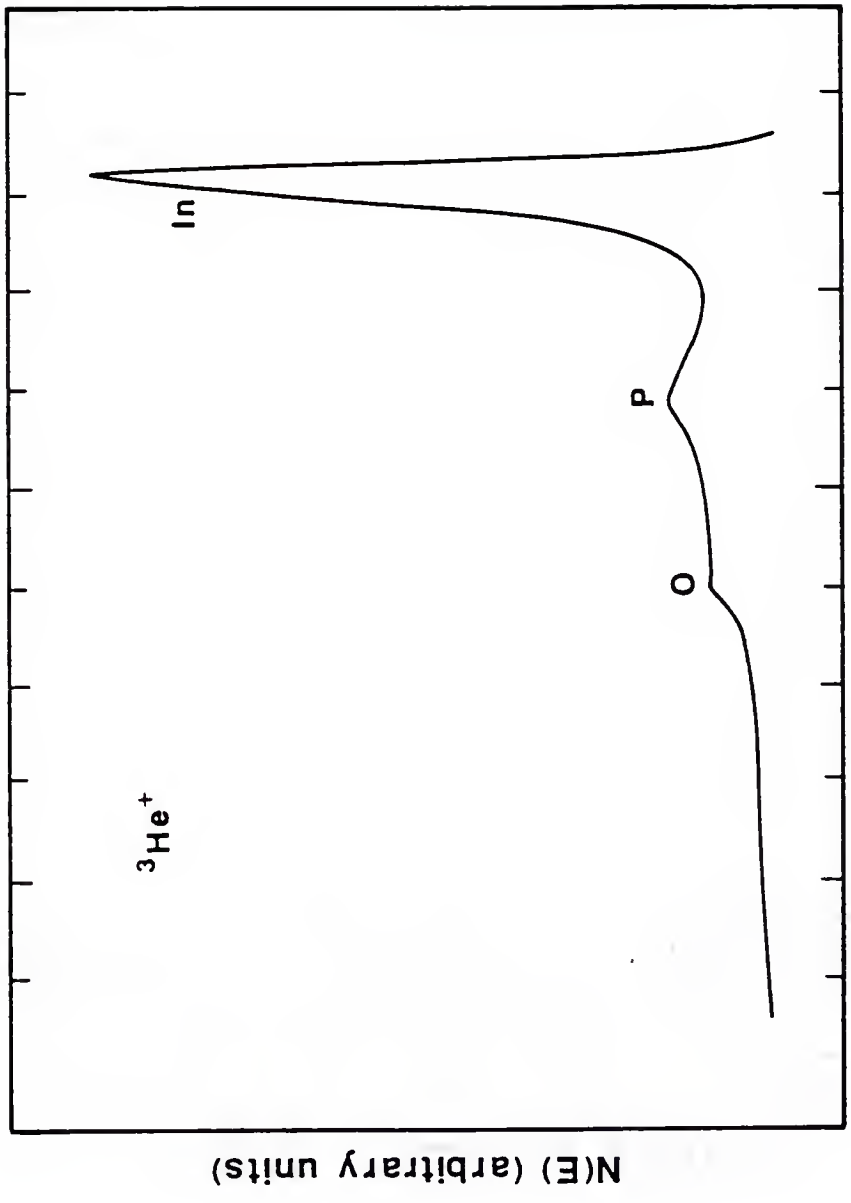

Figure 5-1. ISS spectrum of air-exposed InP(111).

comprise the background and, hence, the magnitude of the background depends upon the electron mobility in the near-surface region. Based on previous ISS studies, it appears that electrons in the surface region of this oxide layer are not highly mobile since the background is fairly large. The elastic scattering cross section increases as the mass of the surface atom increases. Even though In is heavier than P, the size of the In peak indicates that the outermost layer consists predominantly (>80%) of In atoms with roughly equal amounts of O and P atoms. No feature due to surface C appears.

Figure 5-2 shows an angle-integrated AES spectrum of the same surface. An intensity analysis using standard methods[164] yields an In/P atomic concentration ratio which is slightly greater than 1 but much less than the In/P ratio obtained in ISS. This is due to the fact that AES is much less surface sensitive than ISS. The Auger signal is an exponentially weighted average from electrons originating within about three mean-free paths of the sample surface. Since ISS reveals that the outermost layer is mostly In and AES shows that the outermost few layers contain approximately equal amounts of In and P, the one- or two-layer region below the outermost region must be P rich. Both C and O appear in this spectrum in approximately equal concentrations even though no C is detected by ISS at the surface. High resolution AES spectra of the dominant In peaks at a kinetic energy of about 400 eV are shown in figure 5-3. Spectrum (a) was taken at an exit angle of 10° and spectrum (c) was taken at an exit angle of 85°. Spectrum (b) is angle integrated.

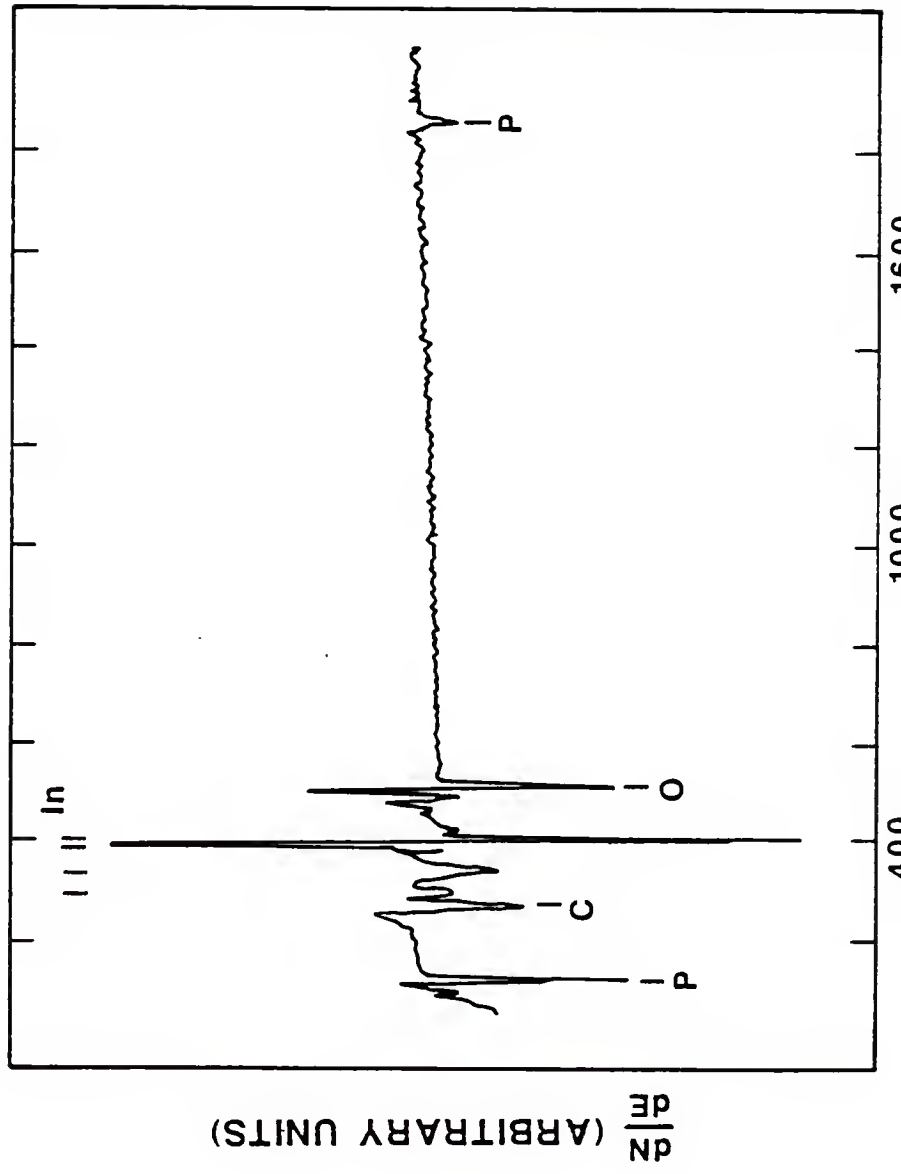

Figure 5-2. Angle-integrated AES spectrum of the same surface shown in figure 5-1.

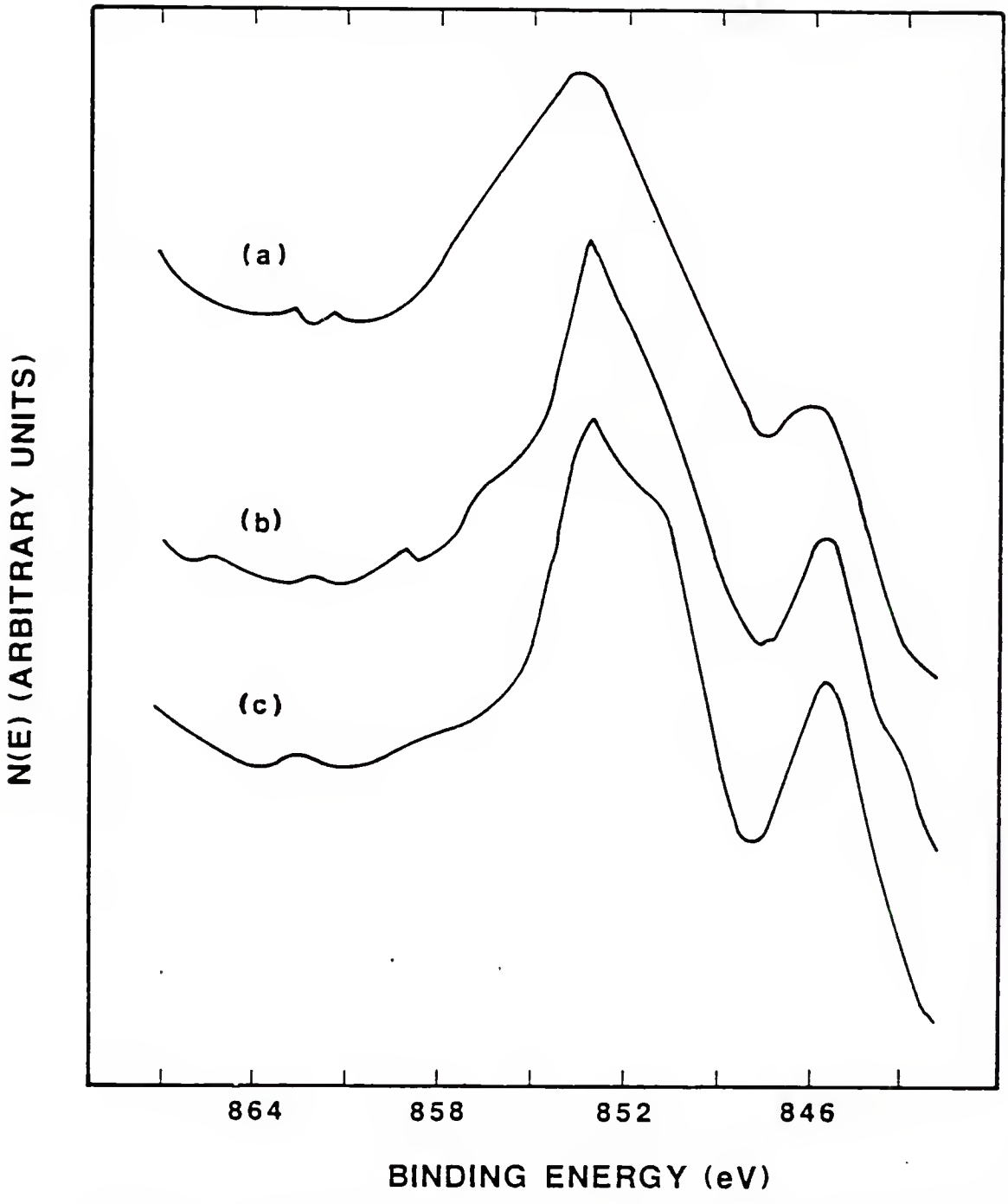

Figure 5-3. AES spectra of the In $M_{4,5}N_{45}N_{45}$ features taken from the same surface shown in figure 5-2. Spectra (a) and (c) were taken at exit angles of 10° and 85° respectively. Spectrum (b) is angle integrated over all exit angles.

These data were taken in the pulse-counting mode and are appropriately referenced so that the energy values are accurate. The spectrum shown in (c) is quite similar in shape to that of In metal[165] and is taken to be representative of InP since most of these electrons are originating deeply below the surface. The kinetic energy of the $M_5N_{45}N_{45}$ transition is 400.6 eV which is about 2.0 eV smaller than values reported for In metal.[165,166] This value is also about 0.6 eV larger than values reported for In_2O_3[166] and agrees with the value found by Clark et al.[151] for InP. Spectrum (a) is much broader and less well defined in comparison with spectrum (c). Based on mean-free path estimates, most of these electrons originate within 10Å of the surface since the exit angle is only 10°. It appears that another set of peaks due to another In species is contained in spectrum (a). The kinetic energy of the $M_5N_{45}N_{45}$ transition for this species is about 397.1 eV. It is argued below that this species is a phosphate and probably $InPO_3$ rather than $InPO_4$. Even though the outermost layer is mostly In, it is probably bonded as $InPO_3$ which is present in an amount almost as large as the amount of InP in the near-surface region. Spectrum (a) is similar to the high-resolution AES spectrum of the primary In features of an InP(100) surface which was etched in a 20% solution of $Br_2/HBr/H_2O$ (1:17:35).[151]

Figures 5-4 and 5-5 show high resolution XPS spectra of the P 2p, In 3d, C 1s and O 1s peaks at exit angles of 10° and 85°. A very large difference is seen between spectra taken at 10° and 85° for the P 2p peaks. The major P 2p feature observed at 129 eV in figure 5-

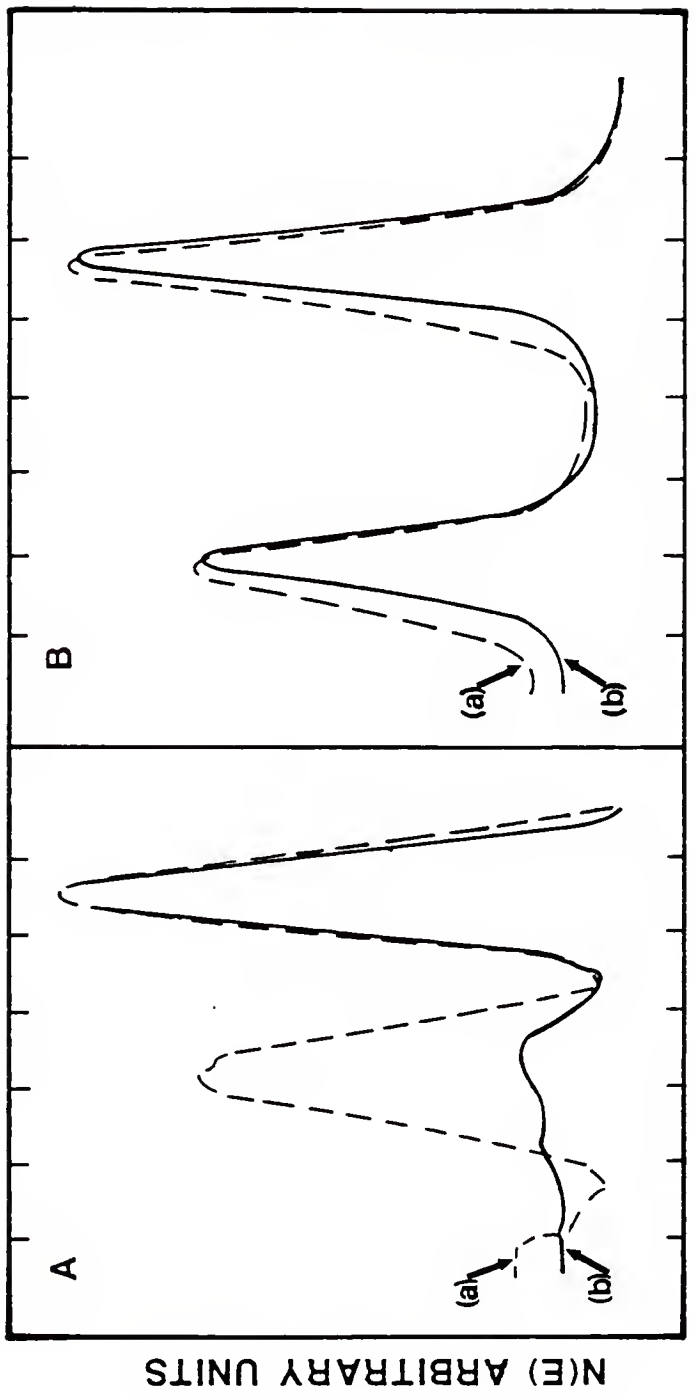

Figure 5-4. XPS spectra of the (A) P 2p and (B) In 3d peaks taken at exit angles of (a) 10° and (b) 85°.

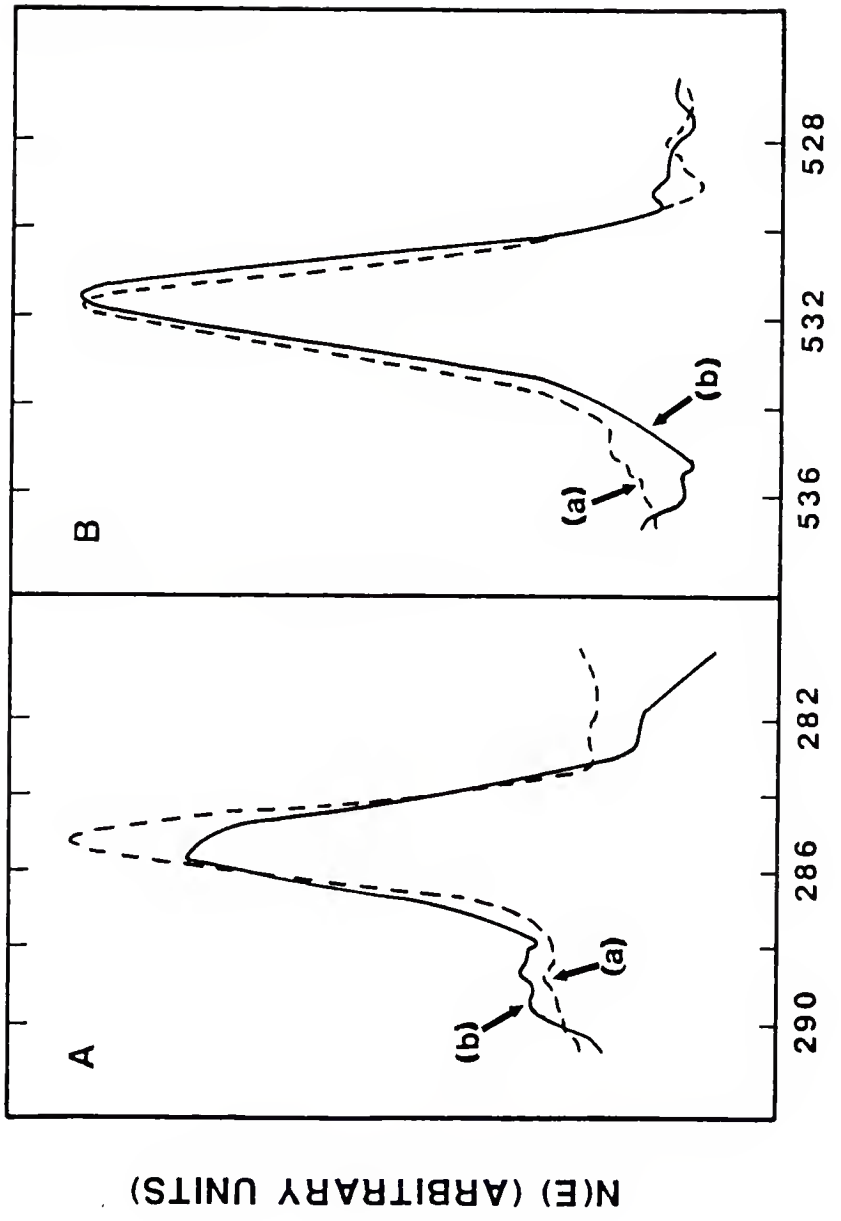

Figure 5-5. XPS spectra of the (A) C 1s and (B) O 1s peaks taken at exit angles of (a) 10° and (b) 85°.

4A(b) is assigned as phosphorous in InP. This is in agreement with other studies[144,147,151,152] and the value assigned to P 2p in GaP.[166] At the surface-sensitive exit angle of 10° shown in figure 5-4A(a), another P 2p peak appears at a binding energy of 133.7 eV which is nearly as large as the P peak due to InP. This is assigned as a phosphate species and probably is $InPO_3$ (or $InPO_4$), but it is difficult to rule out the presence of hydrogen-containing phosphate species. The assignment as $InPO_3$ seems somewhat more probable than $InPO_4$ based on an analogy with $NaPO_3$ or $(NaPO_3)_3$ and Na_3PO_4 which have binding energies of 134, 133.5 and 132.2 eV respectively.[166] A study of the In-P-O phase diagram by Schwartz et al.[167] also suggests that $InPO_3$ forms at low temperatures while $InPO_4$ is stable at elevated temperatures (>650 °C). Based on mean-free path arguments, it is estimated that about 95% of the electrons collected are emitted within 50A of the surface in the 85° exit-angle spectra and within 10A of the surface in the 10° exit-angle spectra. Thus, the spectra shown in figure 5-4A imply that the near-surface region is composed of InP and $InPO_3$ in similar amounts and that the bulk is InP. The In 3d spectra shown in figure 5-4B support this hypothesis. The spectrum shown in (b) is characteristic of In in InP at a binding energy of 444.7 eV. The surface-sensitive spectrum shown in figure 5-4B(a) contains another In species which is assumed to be a phosphate at a binding energy of about 445.5 eV.[147] This is based on the information about P contained in figure 5-4A(a). In in In_2O_3 has a 3d binding energy which is about equal to that of In in InP so it

is not possible to determine if In_2O_3 is present from the spectra shown in figure 5-4.

The C 1s and O 1s XPS features are shown in figure 5-5A and B respectively for exit angles of (a) 10° and (b) 85°. The C 1s peak lies at a binding energy of 285.2 eV, in agreement with Hollinger et al.[168] and is most likely in the form of graphite or hydrocarbons. It should be noted that this binding energy is about 0.6 eV higher than the commonly reported reference values for these species.[166] Therefore, selecting carbon as the reference for peak energy assignments at a binding energy of 284.6 eV would shift all the values reported here to lower binding energies by 0.6 eV. The C 1s peak shown in figure 5-5A(b) is broader than that shown in (a) so more than one form of C may be present. It is possible that discrepancies in the C 1s peak position are due to charging effects. However, these are believed to be minimal for the sample used in this study due to its relatively high conductivity and the thinness of the oxide layer.

XPS O 1s peaks are shown in figure 5-5B. These peaks are discussed assuming that they are composed of a peak due to phosphate at a binding energy of 532.0 eV and a peak due to In_2O_3 at a binding energy of 530.5 eV. This seems reasonable with respect to both the results of this analysis and previous studies.[144,147,152] The surface-sensitive spectrum shown in figure 5-5B(a) is almost entirely due to phosphate. However, the presence of a very small shoulder on the low binding energy side, which is difficult to discern in the

figure, may indicate that a very small amount of In_2O_3 is present in the near-surface region. The more bulk-sensitive spectrum shown in figure 5-5B(b) shows a very slight shift to lower binding energy. This may indicate that the concentration of In_2O_3 is greater with respect to the phosphate at increasing depth below the surface, but the majority of oxygen-containing species throughout the oxide layer is phosphate.

Angle-resolved valence band XPS spectra are shown in figure 5-6. The features of the bulk-sensitive spectrum shown in figure 5-6(b) are in complete agreement with those shown in the spectrum presented by Vesely and Kingston[169] for clean InP. Vesely and Kingston found good agreement between the experimental spectrum and the theoretical results of Stukel et al.[170] and Kramer et al.[171] The characters of the peaks are assigned as: 3 eV - In 5s, 7 eV - O 2p and 9.7 eV - P 3p, and other peaks which are not shown are assigned as: 14 eV - P 3s, 18 eV - In 4d, 23 eV - O 2s.[166,172] The surface-sensitive spectrum shown in figure 5-6(a) is quite similar to the spectrum shown in figure 5-6(b) in the 5 to 12 eV region. However, the broad feature at about 3 eV due to In 5s electrons is absent in the surface-sensitive spectrum. This implies that In is bonded differently in InP than in $InPO_3$.

Depth profiles for In, P, O and C are shown in figure 5-7. These were obtained by performing angle-integrated AES while sputter etching with argon ions. The atomic concentrations were determined using Auger sensitivity factors. However, due to possible matrix

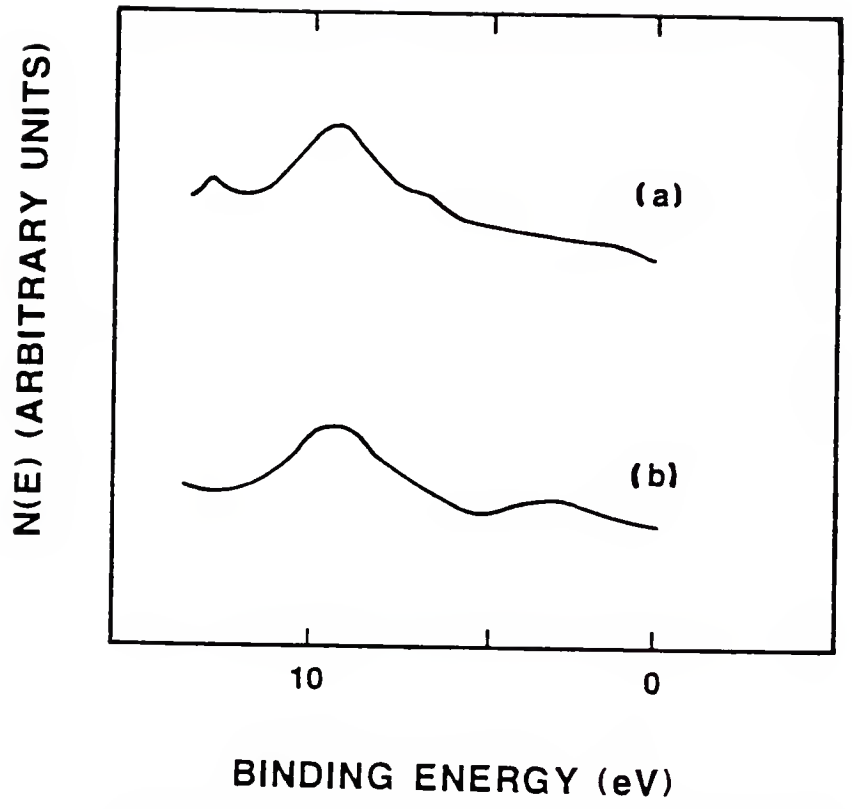

Figure 5-6. Angle-resolved valence band XPS spectra taken at exit angles of (a) 10° and (b) 85°.

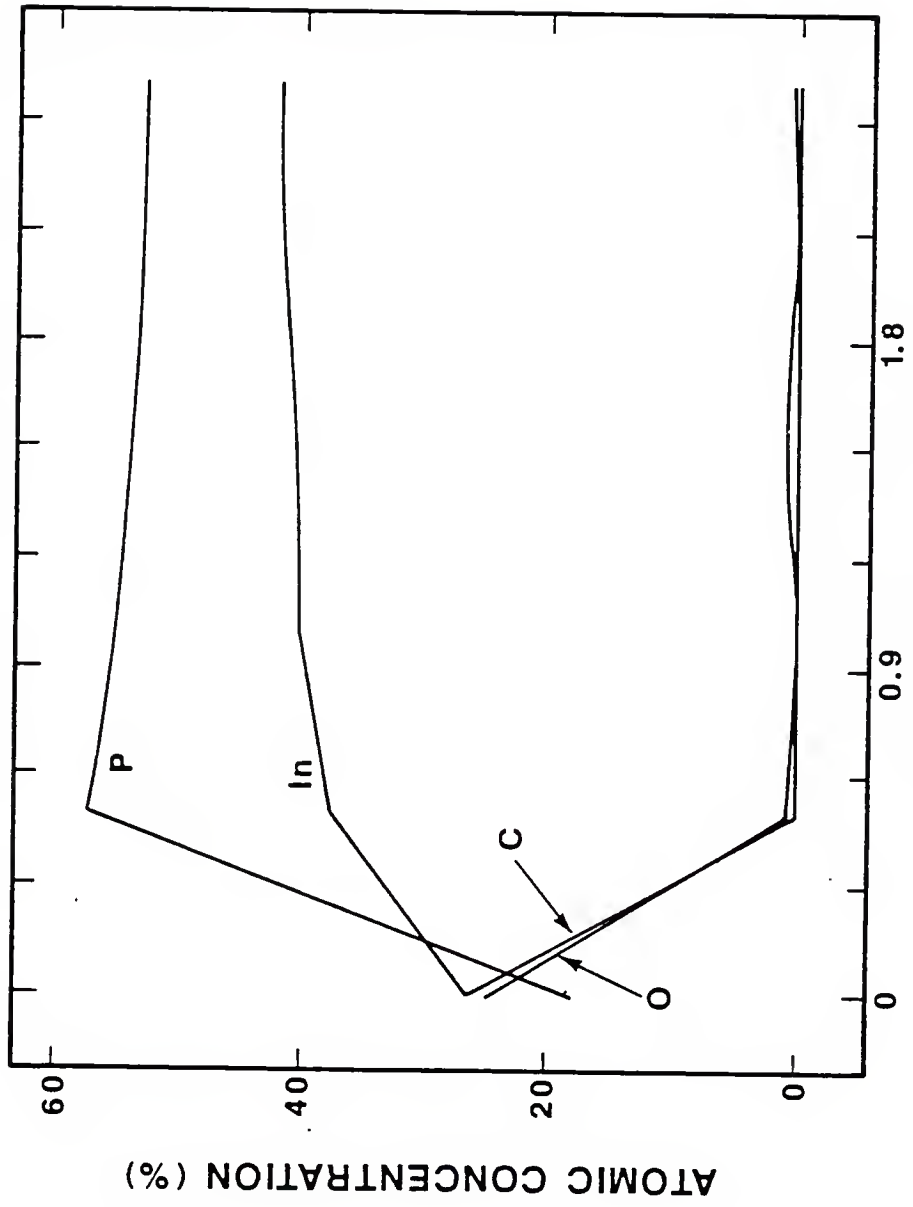

Figure 5-7. Angle-integrated AES compositional profile obtained by argon-ion sputtering.

effects and sputtering artifacts, this figure shows only trends in the concentrations. The profiles are shown as a function of sputter time, but from the angle-resolved XPS results, it is estimated that the sputtering rate was about 50Å/min. The In/P ratio is greater than 1 at the surface, but the large ratio found using ISS is not observed since angle-integrated AES is less surface sensitive than ISS. The P concentration increases rapidly suggesting that the region below the outermost layer is P rich. The In, P, C and O concentrations all change rapidly in the oxide layer, and a sharp interface is observed at a sputtering time of 0.5 minutes. Past this interface only In and P appear. The layer beneath the oxide is P rich, but the concentration of In increases while the concentration of P decreases. Although the In and P concentrations change slowly in this region, it appears that a composition corresponding to InP may be approached.

Conclusions

The oxide layer which forms on a chemically polished and etched InP(111) surface upon exposure to air is very thin (estimated to be about 30Å thick) and nonhomogeneous. ISS shows that the outermost layer is mostly In and AES combined with the ISS results suggests that the region just below the surface layer is P rich. Indium is believed to exist in the near-surface region as $InPO_3$ and InP in similar concentrations, but a very small amount of In_2O_3 is detected in the subsurface region. Carbon is detected throughout the native

oxide layer, and XPS shows that it is present in graphitic or hydrocarbon forms. Depth profiling using Ar^+ and AES shows that the oxide/InP interface is sharply defined. The region below the oxide layer is P rich, but the composition appears to be approaching that of InP as the sputtering time increases.

CHAPTER VI
GENERAL CONCLUSIONS AND RECOMMENDATIONS FOR FUTURE RESEARCH

Hydrogen is found to be present on cleaned and oxidized Si(100) and GaAs(100) as well as cleaned and nitrogen-exposed Si(111). The source of the surface hydrogen detected using ESD is the bulk of the semiconductor which acquires hydrogen during growth, polishing and/or cleaning processes. It would be helpful to substitute deuterium where possible in the formation of the polished single crystal wafers to determine the step(s) during which hydrogen is incorporated.

ESD is one of the relatively few surface analytical techniques which detects hydrogen directly. Energy analysis of the desorbing ions is very useful in distinguishing between different surface binding sites of hydrogen. It was found that multiple states of adsorbed hydrogen are present on cleaned and oxidized Si(100). The ESD study of the Si(100) surface also revealed that the sample treatment can dramatically alter the energy distribution of the desorbing hydrogen ions. Electron beam exposure results in a depopulation of higher energy desorption states which are repopulated upon annealing. Oxygen exposure results in a more marked depopulation of the higher energy desorption states. It was also found from energy-resolved, angle-resolved ESD spectra that different hydrogen bonding states desorb at different angles relative to the surface plane with differing energy distributions. Further research

is necessary to more fully characterize the states of adsorbed hydrogen on the cleaned and oxidized Si(100) surface. ESD threshold studies would be helpful in this endeavor.

In the ISS and TPD study of the interaction between nitrogen and a Si(111)(7x7) surface, ISS easily detects adsorbed nitrogen following doses as low as 2 L and reveals that a saturation dose of N_2 at room temperature is 75 L. Using TPD, evidence of at least two chemisorbed states of nitrogen is found. Hydrogen, which originates from the bulk of the sample, is found to associate with the surface nitrogen. No adsorbed nitrogen is detected using AES for doses as high as 3000 L. Angle-resolved AES, a technique developed by Hoflund[173] which allows for greatly enhanced surface sensitivity using AES, may be useful in determining whether the nitrogen is present only on the surface or penetrates into the silicon.

From the ESD study of the GaAs(100), it was verified that molecular deuterium does not adsorb at significant rates at room temperature on the cleaned or oxidized surface, but that it does adsorb on both surfaces when the sample is subjected to radiant heating in the range 200-400 °C. There appears to be two states of hydrogen on oxidized GaAs(100). There also appears to be two states on the cleaned GaAs(100) surface, but the higher energy state has a lower desorption cross section or is less densely populated. ESD gives a relative measure of the amount of adsorbed deuterium. Again, further research is needed to fully characterize the states of hydrogen on the surface.

The native oxide layer present on chemicallly poslished and etched InP(111) is approximately 30Å thick. A sharp interface exists between the oxide and the bulk InP. ISS reveals that the outermost atomic layer is In rich, and AES combined with the ISS shows that the region beneath this is P rich. InP and $InPO_3$ are present in approximately equal concentrations, and a small amount of In_2O_3 is detected. Carbon is present throughout the oxide layer as graphite and/or hydrocarbons. Similar studies of native oxide layers formed under different polishing and/or etching conditions would be useful. Additionally, it is suspected that hydrogen is present in the oxide layer. It would be interesting to perform an ESD study to determine whether or not this is true and to characterize the hydrogen.

The studies performed have been successful in obtaining an understanding of a number of interactions between gases and semiconductors. Further research would be helpful in gaining a more thorough understanding of these interactions. Ultimately, it is also very important to correlate the information gained using surface analytical techniques with a characterization of the electronic properties of the systems studied.

REFERENCES

1. G.B. Hoflund, D.F. Cox, G.L. Woodson and H.A. Laitinen, Thin Solid Films 78, 357 (1981).

2. C.H. Seager and D.S. Ginley, Appl. Phys. Lett. 34, 337 (1979).

3. J.L. Benton, C.J. Doherty, S.D. Ferris, D.L. Flamm, L.C. Kimerling and H.J. Leamy, Appl. Phys. Lett. 36, 670 (1980).

4. S.J. Pearton and A.J. Tavendale, Phys. Rev. B 26, 7105 (1982).

5. C.-T. Sah, J.Y.-C. Sun and J.J.-T. Tzou, Appl. Phys. Lett. 43, 204 (1983).

6. C.-T. Sah, J.Y.-C. Sun and J.J.-T. Tzou, J. Appl. Phys. 54, 5864 (1983).

7. J.I. Pankove, D.E. Carlson, J.E. Berkeyheiser and R.O. Wance, Phys. Rev. Lett. 51, 2224 (1983).

8. W.L. Hansen, S.J. Pearton and E.E. Haller, Appl. Phys. Lett. 44, 606 (1984).

9. J.I. Pankove, R.O. Wance and J.E. Berkeyheiser, Appl. Phys. Lett. 45, 1100 (1984).

10. N.M. Johnson, Phys. Rev. B 31, 5525 (1985).

11. J.I. Pankove, P.J. Zanzucchi, C.W. Magee and G. Lucovsky, Appl. Phys. Lett. 46, 421 (1985).

12. N.M. Johnson and M.D. Moyer, Appl. Phys. Lett. 46, 787 (1985).

13. S.J. Pearton, Appl. Phys. Lett. 40, 253 (1982).

14. J. Lagowski, M. Kaminska, J.M. Parsey, H.C. Gatos and M. Lichtensteiger, Appl. Phys. Lett. 41, 1078 (1982).

15. S.J. Pearton, J. Appl. Phys. 53, 4509 (1982).

16. J. Chevallier, W.C. Dautremont-Smith, C.W. Tu and S.J. Pearton, Appl. Phys. Lett. 47, 108 (1985).

17. S.J. Pearton, W.C. Dautremont-Smith, J. Chevallier, C.W. Tu and K.D. Cummings, J. Appl. Phys. 59, 2821 (1986).

18. Y.-C. Pao, D. Liu, W.S. Lee and J.S. Harris, Appl. Phys. Lett. 48, 1291 (1986).

19. M.M. Moslehi and K.C. Saraswat, IEEE Trans. Electron. Devices ED-32, 106 (1985).

20. L. Messick, J. Appl. Phys. 47, 4949 (1976).

21. D. Fritsche, Electron Lett. 14, 51 (1978).

22. L. Meiners, J. Vac. Sci. Technol. 19, 373 (1981).

23. T. Kawakami and M. Okamura, Electron Lett. 15, 502 (1979).

24. J. Magarino, D. Kaplan, A. Friederich and A. Deneuville, Philos. Mag. B 45, 285 (1982).

25. G.G. LeLeo and W.B. Fowler, J. Electron. Mater. 14a, 745 (1985).

26. T. Sakurai and H.D. Hagstrum, Phys. Rev. B 14, 1593 (1976).

27. K.C. Pandey, J. Vac. Sci. Technol. 15, 440 (1978).

28. W. Mönch , P. Koke and S. Krueger, J. Vac. Sci. Technol. 19, 313 (1981).

29. K. Fujiwara, Phys. Rev. B 26, 2036 (1982).

30. N.G. Norton, Vacuum 33, 621 (1983).

31. H. Froitzheim, U. Köhler and H. Lammering, Surf. Sci. 149, 537 (1985).

32. N.D. Lang and A.R. Williams, Phys. Rev. Lett. 34, 531 (1975).

33. J.A. Appelbaum and D.R. Hamann, Phys. Rev. Lett. 34, 806 (1975).

34. I.P. Batra and S. Ciraci, Phys. Rev. Lett. 34, 1337 (1975).

35. K.C. Pandey, Phys. Rev. B 14, 1557 (1976).

36. I.P. Batra, S. Ciraci and I.B. Ortenburger, Solid State Commun. 18, 563 (1976).

37. K.M. Ho, M.L. Cohen and M. Schlüter , Phys. Rev. B 15, 3888 (1977).

38. J.A. Appelbaum, D.R. Hamann and K.H. Tasso, Phys. Rev. Lett. 39, 1487 (1977).

39. J.A. Appelbaum, G.A. Baraff, D.R. Hamann, H.D. Hagstrum and T. Sakurai, Surf. Sci. 70, 654 (1978).

40. W.Y. Ching, D.J. Lam and C.C. Lin, Phys. Rev. B 21, 2378 (1980).

41. H. Ibach and J.E. Rowe, Surf. Sci. 43, 481 (1974).

42. J.E. Rowe, Surf. Sci. 53, 461 (1975).

43. T. Sakurai and H.D. Hagstrum, Phys. Rev. B 12, 5349 (1975).

44. K.C. Pandey, T. Sakurai and H.D. Hagstrum, Phys. Rev. Lett. 35, 1728 (1975).

45. H. Froitzheim, H. Ibach and S. Lehwald, Phys. Lett. 55A, 247 (1975).

46. T. Sakurai, K.C. Pandey and H.D. Hagstrum, Phys. Lett. 56A, 204 (1976).

47. T. Sakurai and H.D. Hagstrum, J. Vac. Sci. Technol. 13, 807 (1976).

48. S.J. White and D.P. Woodruff, J. Phys. C9, L451 (1976).

49. S.J. White and D.P. Woodruff, Surf. Sci. 63, 254 (1977).

50. T. Sakurai, T.T. Tsong and R.J. Culbertson, J. Vac. Sci. Technol. 15, 647 (1978).

51. S.J. White, D.P. Woodruff and L. McDonnell, Surf. Sci. 72, 77 (1978).

52. S.J. White, D.P. Woodruff, B.W. Holland and R.S. Zimmer, Surf. Sci. 74, 34 (1978).

53. L.C. Feldman, P.J. Silverman and I. Stensgaard, Nucl. Instr. Methods 168, 589 (1980).

54. H.H. Madden, Surf. Sci. 105, 129 (1981).

55. H. Wagner, R. Butz, U. Backes and D. Bruchmann, Solid State Commun. 38, 1155 (1981).

56. H.H. Madden, D.R. Jennison, M.M. Traum, G. Margaritondo and N.G. Stoffel, Phys. Rev. B 26, 896 (1982).

57. S. Maruno, H. Iwasaki, K. Horioka, S.-T. Li and S. Nakamura, Surf. Sci. 123, 18 (1982).

58. T.S. Shi, S.N. Sahu, G.S. Oehrlein, A. Hiraki and J.W. Corbett, Phys. Stat. Sol. 74, 329 (1982).

59. S. Maruno, H. Iwasaki, K. Horioka, S.-T. Li and S. Nakamura, Phys. Rev. B 27, 4110 (1983).

60. H.H. Madden, J. Vac. Sci. Technol. A 2, 961 (1984).

61. J.A. Schaefer, F. Stucki, J.A. Anderson, G.J. Lapeyre and W. Gopel, Surf. Sci. 140, 207 (1984).

62. D. Schmeisser, Surf. Sci. 137, 197 (1984).

63. Y.J. Chabal, J. Vac. Sci. Technol A 3, 1448 (1985).

64. Y.J. Chabal and K. Raghavachari, Phys. Rev. Lett. 54, 1055 (1985).

65. M. Nishijima, K. Edamoto, Y. Kubota, H. Kobayashi and M. Onchi, Surf. Sci. 158, 422 (1985).

66. C. Kleint, Vacuum 36, 267 (1986).

67. L.L. Kazmerski, in Eighteenth IEEE Photovoltaic Specialists Conference (1985), p. 993.

68. C.F. Corallo and G.B. Hoflund, J. Vac. Sci. Technol. A 5, 713 (1987).

69. M.M. Traum and D.P. Woodruff, J. Vac. Sci. Technol. 17, 1202 (1980).

70. G.B. Hoflund, SEM J. 4, 1391 (1985).

71. R. Jaeger, J. Stöhr and T. Kendelewicz, Phys. Rev. B 28, 1145 (1983).

72. J.W. Corbett, S.N. Sahu, T.S. Shi and L.C. Snyder, Phys. Lett. 93A, 303 (1983).

73. J.S. Johannessen and W.E. Spicer, Thin Solid Films 32, 311 (1976).

74. H.G. Maguire and P.D. Augustus, J. Electrochem. Soc. 119, 791 (1972).

75. R. Heckingbottom, G.W.B. Ashwell, P.A. Leigh, S. O'Hara and C.J. Todd, Proc. Electrochem. Soc. 78, 419 (1978).

76. H.H. Madden and P.H. Holloway, J. Vac. Sci. Technol. 16, 618 (1979).

77. N.C. Tombs, F.A. Sewell, Jr. and J.J. Comer, J. Electrochem. Soc. 116, 862 (1969).

78. M.J. Rand and J.F. Roberts, J. Electrochem. Soc. 120, 446 (1973).

79. D.M. Brown, P.V. Gray, F.K. Heumann, H.R. Philipp and E.A. Taft, J. Electrochem. Soc. 115, 311 (1968).

80. A. Atkinson, A.J. Moulson and E.W. Roberts, J. Am. Ceram. Soc. 59, 285 (1976).

81. A. Atkinson, A.J. Moulson and E.W. Roberts, J. Mater. Sci. 10, 1242 (1975).

82. S.M. Hu, J. Electrochem. Soc. 113, 693 (1966).

83. R.G. Frieser, J. Electrochem. Soc. 115, 1902 (1968).

84. M.I. Kamchatka and B.F. Ormont, Russian J. Phys. Chem. 45, 1246 (1971).

85. T. Ito, T. Nozaki, T. Nakamura and H. Hishikawa, Appl. Phys. Lett. 38, 370 (1981).

86. T. Ito, S. Hijiya, H. Arakawa, T. Nozaki, M. Shinoda and Y. Fukukawa, J. Electrochem. Soc. 125, 449 (1978).

87. T. Ito, T. Nozaki, H. Arakawa and M. Shinoda, Appl. Phys. Lett. 32, 330 (1978).

88. S.M. Murarka, C.C. Chang and A.C. Adams, J. Electrochem. Soc. 126, 996 (1979).

89. A.G. Schrott and S.C. Fain, Jr., Surf. Sci. 111, 39 (1981).

90. A.G. Schrott and S.C. Fain, Jr., Surf. Sci. 123, 204 (1982).

91. J.F. Delord, A.G. Schrott and S.C. Fain, Jr., J. Vac. Sci. Technol. 17, 517 (1980).

92. C. Maillot, H. Roulet and G. Dufour, J. Vac. Sci. Technol. B 2, 316 (1984).

93. K. Edamoto, S. Tanaka, M. Onchi and M. Nishijima, Surf. Sci. 167, 285 (1986).

94. J.A. Taylor, G.M. Lancaster, A. Igniatiev and J.W. Rabalais, J. Chem. Phys. 68, 1776 (1978).

95. R. Heckingbottom, The Structure and Chemistry of Solid Surfaces, edited by G.A. Somorjai (Wiley, New York, 1969), p. 78-1.

96. R.B. Guthrie and F.L. Riley, Proc. Br. Ceram. Soc. 22, 275 (1973).

97. M.D. Wiggins, R.J. Baird and P. Wynblatt, J. Vac. Sci. Technol. 18, 965 (1981).

98. R. Heckingbottom and P.R. Wood, Surf. Sci. 36, 594 (1973).

99. A.J. van Bommel and F. Meyer, Surf. Sci. 8, 381 (1967).

100. A. Glachant, D. Saidi and J.F. Delord, Surf. Sci. 168, 672 (1986).

101. M. Nishijima, K. Edamoto, Y. Kubota, H. Kobayashi and M. Onchi, Surf. Sci. 158, 422 (1985).

102. D.-R. He and F.W. Smith, Surf. Sci. 154, 347 (1985).

103. E.G. Keim and A. van Silfhout, Surf. Sci. 152, 1096 (1985).

104. T.M. Buck, Methods of Surface Analysis: Methods and Phenomena I, edited by A.W. Czanderna (Elsevier Scientific, Amsterdam, 1975), p. 75.

105. E.P.Th.M. Suurmeijer and A.L. Boers, Surf. Sci. 43, 309 (1973).

106. E.S. Parilis in Proc. 7th Intern. Conf. Phenomena in Ionized Gases, Belgrade (1965), p. 129.

107. J. Onsgaard, W. Heiland and E. Taglauer, Surf. Sci. 99, 112 (1980).

108. H.F. Dylla, J.G. King and M.J. Cardillo, Surf. Sci. 74, 141 (1978).

109. R.P.H. Gasser, An Introduction to Chemisorption and Catalysis (Oxford Science, Oxford, 1985), Chpt. 3.

110. C.F. Corallo and G.B. Hoflund, unpublished manuscript.

111. R.C. Weast (ed.) CRC Handbook of Chemistry and Physics, (CRC Press, Boca Raton, FL, 1979-80).

112. J.F. O'Hanlon, A User's Guide to Vacuum Technology (Wiley, New York, 1980), Appendix E.

113. A. Cornu and R. Massot, Compilation of Mass Spectral Data (Heyden & Sons Ltd., London, 1975), Vol. 2.

114. A.R. Calawa, Appl. Phys. Lett. 33, 1020 (1978).

115. H. Mori and S. Takagishi, Jap. J. Appl. Phys. 23, L877 (1984).

116. P.D. Dapkus, H.M. Manasevit and K.L. Hess, J. Cryst. Growth 55, 10 (1981).

117. E. Veuhoff, W. Pletsheu, P. Balk and H. Lüth, J. Cryst. Growth 55, 30 (1981).

118. L.M. Fraas, J. Appl. Phys. 52, 6939 (1981).

119. P. Friedel and S. Gourrier, Appl. Phys. Lett. 42, 509 (1983).

120. R.P.H. Chang and S. Darack, Appl. Phys. Lett. 38, 898 (1981).

121. P. Friedel, P.K. Larsen, A. Gourrier, J.P. Cabanie and W.M. Gerits, J. Vac. Sci. Technol. B 2, 675 (1984).

122. D.D. Pretzer and H.D. Hagstrum, Surf. Sci. 4, 265 (1966).

123. P.E. Gregory and W.E. Spicer, Surf. Sci. 54, 229 (1976).

124. P.E. Gregory and W.E. Spicer, Phys. Rev. B 12, 2370 (1975).

125. W. Mokwa, D. Kohl and G. Heiland, Phys. Rev. B 29, 6709 (1984).

126. H. Lüth and R. Matz, Phys. Rev. Lett. 46, 1652 (1981).

127. L.H. Dubois and G.P. Schwartz, Phys. Rev. B 26, 794 (1982).

128. F. Bartels, L. Surkamp, H.J. Clemens and W. Mönch, J. Vac. Sci. Technol. B 1, 756 (1983).

129. W. Mönch, Thin Solid Films 104, 285 (1983).

130. R.Z. Bachrach, R.S. Bauer, P. Chiaradia and G.V. Hansson, J. Vac. Sci. Technol. 18, 797 (1981).

131. P. Drathen, W. Ranke and K. Jacobi, Surf. Sci. 77, 1162 (1978).

132. R.D. Bringans and R.Z. Bachrach, Physica 117B & 118B, 854 (1983).

133. R.D. Bringans and R.Z. Bachrach, Solid State Commun. 45, 83 (1983).

134. R.D. Bringans and R.Z. Bachrach, J. Vac. Sci. Technol. A 1, 676 (1983).

135. R.Z. Bachrach and R.D. Bringans, J. de Physique C 5, 145 (1982).

136. T.E. Madey and J.T. Yates, Jr., J. Vac. Sci. Technol. 8, 39 (1971).

137. R.E. Gilbert, D.F. Cox and G.B. Hoflund, Rev. Sci. Instrum. 53, 14 (1982).

138. M.L. Knotek, Phys. Today Sept., 24 (1984).

139. T.E. Madey, Surf. Sci. 36, 281 (1973).

140. W. Jelend and D. Menzel, Chem. Phys. Lett. 21, 178 (1973).

141. D.A. King and D. Menzel, Surf. Sci. 40, 399 (1973).

142. R.P. Vasquez, B.F. Lewis and F.J. Grunthaner, Appl. Phys. Lett. 42, 293 (1983).

143. M.G. Dowset and E.H.C. Parker, J. Vac. Sci. Technol. 16, 1207 (1979).

144. A. Nelson, K. Geib and C.W. Wilmsen, J. Appl. Phys. 54, 4134 (1983).

145. M. Yamaguchi and K. Ando, J. Appl. Phys. 51, 5007 (1980).

146. C.W. Wilmsen, K.M. Geib, R. Gann, J. Costello, G. Hrychowian and R.J. Zeto, J. Vac. Sci. Technol. B 3, 1103 (1985).

147. M. Faithpour, P.K. Boyer, G.J. Collins and C.W. Wilmsen, J. Appl. Phys. 57, 637 (1985).

148. L. Koenders, F. Bartels, H. Ulrich and W. Monch, J. Vac. Sci. Technol. B 3, 1107 (1985).

149. G.S. Korotchenkov, V.A. Mikhailov and V.I. Tsvitsinsky, J. Vac. Sci. Technol. B 3, 981 (1985).

150. J. Oliver, P. Faulconnier and R. Poirier, J. Appl. Phys. 51, 4990 (1980).

151. D.T. Clark, T. Fok, G.C. Roberts and R.W. Sykes, Thin Solid Films 70, 261 (1980).

152. J.F. Wager, D.L. Ellsworth, S.M. Goodnick and C.W. Wilmsen, J. Vac. Sci. Techol. 19, 513 (1981).

153. P.A. Bertrand, J. Vac. Sci. Technol. 18, 28 (1981).

154. P.A. Kohl, C. Wolowodiuk and F.W. Ostermayer, Jr., J. Electrochem. Soc. 130, 2288 (1983).

155. C.W. Tu and A.R. Schlier, Appl. Surf. Sci. 11/12, 355 (1982).

156. O. Wada, J. Phys. D: Appl. Phys. 17, 2429 (1984).

157. B. Achard, B. Guzza and C. Pariset, Surf. Sci. 160, L519 (1985).

158. J. Oliver, J. Appl. Phys. 51, 5406 (1980).

159. J. Massies and F. Lamaire-Dezaly, J. Appl. Phys. 55, 3136 (1974).

160. C.R. Bayliss and D.L. Kirk, Thin Solid Films 29, 97 (1975).

161. J. Massies and F. Lamaire-Dezaly, J. Appl. Phys. 57, 237 (1985).

162. S.N.G. Chu, C.M. Jodlauk and W.D. Johnston, Jr., J. Electrochem. Soc. 130, 2398 (1983).

163. D. Daoxuan and Z. Furong, Chin. J. Semicond. 6, 190 (1985).

164. L.E. Davis, N.C. MacDonald, P.W. Palmberg, G.E. Riach and R.E. Weber, Handbook of Auger Electron Spectroscopy (Physical Electronics Industries, Inc., Eden Prairie, MN., 1976).

165. A.C. Parry-Jones, P. Weightman and P.T. Andrews, J. Phys. C: Solid State Phys. 12, 1587 (1979).

166. C.D. Wagner, W.M. Riggs, L.E. Davis, J.F. Moulder and G.E. Muilenberg (eds.) Handbook of X-ray Photoelectron Spectroscopy (Perkin-Elmer Corporation, Eden Prairie, MN., 1979).

167. G.P. Schwartz, W.A. Sunder and J.E. Griffiths, J. Electrochem. Soc. 129, 1361 (1982).

168. G. Hollinger, E. Bergignat, J. Joseph and Y. Robach, J. Vac. Sci. Technol. A 3, 2082 (1985).

169. C.J. Vesely and D.L. Kingston, Phys. Rev. B 8, 2685 (1973).

170. D. Stukel, T. Collins and R. Euwema, Electronic Density of States, edited by L. Bennett (Natl. Bur. Std. Spec. Publ. No. 323, U.S. GPO, Washington, D.C., 1971), p. 93.

171. B. Kramer, K. Maschke and P. Thomas, Phys. Status Solidi B 48, 635 (1971).

172. R.A. Pollak, S. Kowalczyk, L. Ley and D.A. Shirley, Phys. Rev. Lett. 29, 274 (1972).

173. G.B. Hoflund, D.A. Asbury, C.F. Corallo and G.R. Corallo, accepted by J. Vac. Sci. Technol.

BIOGRAPHICAL SKETCH

Cheryl Lee Fox was born on August 6, 1959, in Buffalo, New York. She is the daughter of Franklin J. and Elaine G. Fox and has three sisters and one brother: Laurie, Robin, Dawn and Jeff. Cheryl was married on September 1, 1984, to a fellow graduate student, Gregory R. Corallo.

Cheryl was raised in Buffalo, New York, until the age of fourteen when the family moved to Cheektowaga, New York, a suburb of Buffalo. The family moved to Monroe, North Carolina, when Cheryl was a freshman in high school. She graduated from Parkwood High School in 1977. She then attended Wake Forest University for two years, worked for Celanese Corp. for one year and attended N. C. State University for three years. She received a Bachelor of Science in chemical engineering in 1983 from N. C. State University. Cheryl then entered graduate school in chemical engineering at the University of Florida in September of 1983. She obtained a Master of Science degree in 1984 and continued in the Ph.D. program under the direction of Dr. Gar B. Hoflund where she has been until the present.

I certify that I have read this study and that in my opinion it conforms to acceptable standards of scholarly presentation and is fully adequate, in scope and quality, as a dissertation for the degree of Doctor of Philosophy.

Gar B. Hoflund, Chairman
Professor of Chemical Engineering

I certify that I have read this study and that in my opinion it conforms to acceptable standards of scholarly presentation and is fully adequate, in scope and quality, as a dissertation for the degree of Doctor of Philosophy.

Timothy J. Anderson
Associate Professor of Chemical Engineering

I certify that I have read this study and that in my opinion it conforms to acceptable standards of scholarly presentation and is fully adequate, in scope and quality, as a dissertation for the degree of Doctor of Philosophy.

Vaneica Y. Young
Assistant Professor of Chemistry

This dissertation was submitted to the Graduate Faculty of the College of Engineering and to the Graduate School and was accepted as partial fulfillment of the requirements for the degree of Doctor of Philosophy.

December, 1987

Herbert G. Brewer
Dean, College of Engineering

Dean, Graduate School

UNIVERSITY OF FLORIDA
3 1262 08554 1562